iScience

CellPress

Article

Paracrine Crosstalk between Fibroblasts and ER$^+$ Breast Cancer Cells Creates an IL1β-Enriched Niche that Promotes Tumor Growth

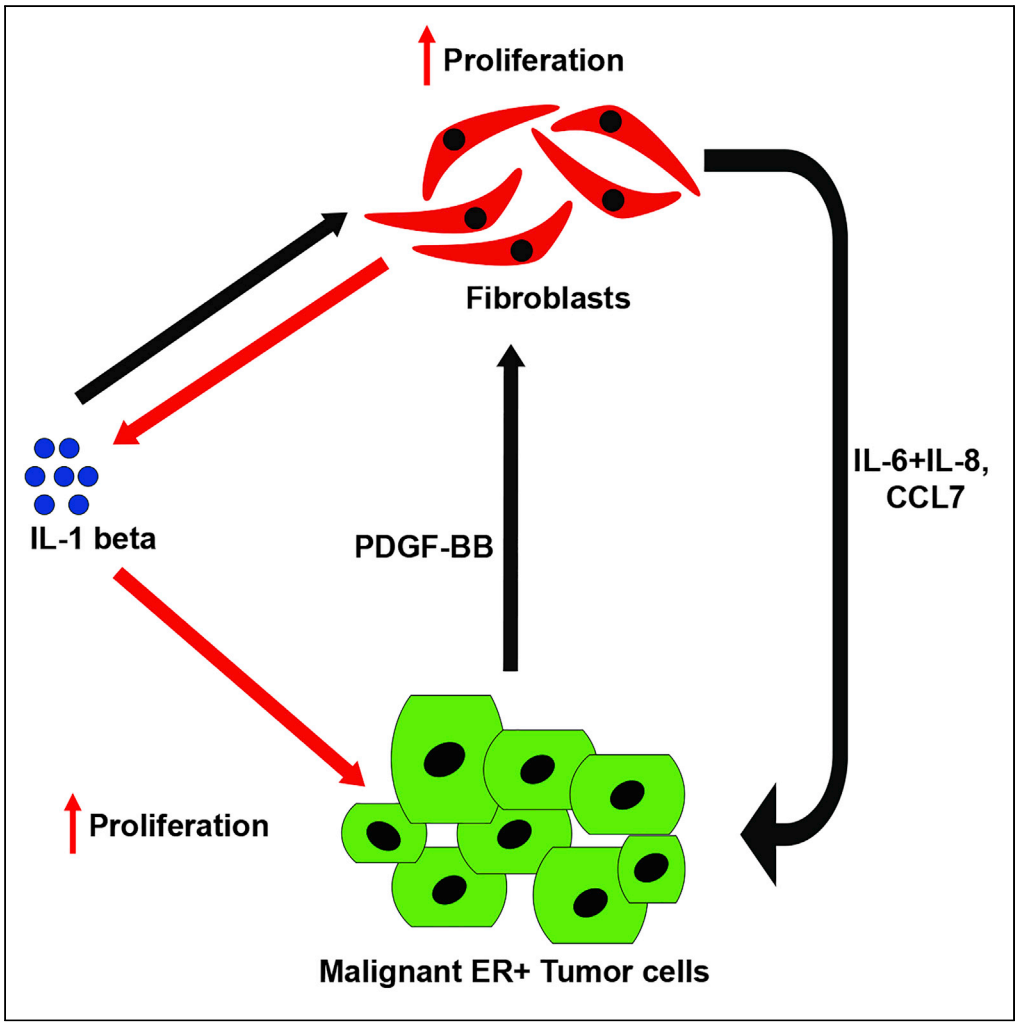

Sumanta Chatterjee, Vasudeva Bhat, Alexei Berdnikov, ..., Leigh C. Murphy, Lynne-Marie Postovit, Afshin Raouf

afshin.raouf@umanitoba.ca

HIGHLIGHTS

Normal fibroblast-cancer cell interaction promotes tumor progression

Paracrine signaling common to normal and activated fibroblasts promotes drug resistance

Fibroblast-secreted factors create an IL1β-enriched niche for ER$^+$ breast cancer cell growth

Chatterjee et al., iScience *19*, 388–401
September 27, 2019
https://doi.org/10.1016/j.isci.2019.07.034

iScience

CellPress

Article

Paracrine Crosstalk between Fibroblasts and ER$^+$ Breast Cancer Cells Creates an IL1β-Enriched Niche that Promotes Tumor Growth

Sumanta Chatterjee,[1,2] Vasudeva Bhat,[1,2] Alexei Berdnikov,[3] Jiahui Liu,[6] Guihua Zhang,[6] Edward Buchel,[3] Janice Safneck,[4] Aaron J. Marshall,[1] Leigh C. Murphy,[2,5] Lynne-Marie Postovit,[6,7] and Afshin Raouf[1,2,8,*]

SUMMARY

Breast cancer-induced activated fibroblasts support tumor progression. However, the role of normal fibroblasts in tumor progression remains controversial. In this study, we used modified patient-derived organoid cultures and demonstrate that constitutively secreted cytokines from normal breast fibroblasts initiate a paracrine signaling mechanism with estrogen receptor-positive (ER$^+$) breast cancer cells, which results in the creation of an interleukin (IL)-1β-enriched microenvironment. We found that this paracrine signaling mechanism is shared between normal and activated fibroblasts. Interestingly, we observed that in reconstructed tumor microenvironment containing autologous ER$^+$ breast cancer cells, activated fibroblasts, and immune cells, tamoxifen is more effective in reducing tumor cell proliferation when this paracrine signaling is blocked. Our findings then suggest that ER$^+$ tumor cells could create a growth-promoting environment without activating stromal fibroblasts and that in breast-conserving surgeries, normal fibroblasts could be a significant modulator of tumor recurrence by enhancing the proliferation of residual breast cancer cells in the tumor-adjacent breast tissue.

INTRODUCTION

Current evidence suggests that cancer initiation and progression is co-mediated by the tissue environment (niche) and cancer cells rather than being a cell-autonomous-driven process (Guarnerio et al., 2018; Hanahan and Weinberg, 2011; Plaks et al., 2015). The breast cancer tumor niche consists of stromal and extracellular matrix (ECM) components, which form a complex network enabling tumor cells to maintain growth and proliferation to develop invasive and metastatic phenotypes (Acharyya et al., 2012; Lu et al., 2014; Quail and Joyce, 2013). Fibroblasts, a major stromal component of the tumor niche, have been identified as an important modifier of tumor progression (Cohen et al., 2017; Erez et al., 2010; Otomo et al., 2014). In normal breast tissue, the role of fibroblasts is to provide ECM; secrete cytokines and growth factors to support the proliferation, differentiation, and self-renewal of the epithelial stem and progenitor cells; regulate inflammatory responses; and participate in wound healing (Chatterjee et al., 2015, 2018; Makarem et al., 2013). In the tumor niche, however, a subpopulation of fibroblasts called tumor-associated fibroblasts (TAFs) have been implicated in promoting tumor cell proliferation and cancer progression (Bussard et al., 2016; Gascard and Tlsty, 2016). These TAFs have acquired a modified and activated phenotype that is identified based on their expression of alpha-smooth muscle actin and the fibroblast activation protein (Allaoui et al., 2016; Yang et al., 2016). The activated fibroblasts make up about 40%–80% of breast tumor stroma (Bhowmick et al., 2004; Chatterjee et al., 2018; Karnoub et al., 2007; Orimo et al., 2005). Extensive studies regarding the interactions between the TAFs and breast cancer cells (BCCs) have revealed a cyclic relationship in which cancer cells stimulate a reactive response in fibroblasts and in turn activated fibroblasts enhance the proliferation and migration of cancer cells. In this regard, the secretion of transforming growth factor (TGF)-β and CXCL12 by the cancer cells has been suggested as one mechanism to confer the activated phenotype in normal stromal fibroblasts. Activated fibroblasts in turn through secretion of fibroblast growth factors, hepatocyte growth factor, interleukin (IL) 6, and TGF-β enhance cancer progression and tumor metastasis (Boimel et al., 2012; Chatterjee et al., 2018; Hugo et al., 2012; Kuperwasser et al., 2004; Pickup et al., 2013; Scherz-Shouval et al., 2014; Sharon et al., 2015).

In contrast, much less is known about the nature of interaction between BCCs and normal stromal fibroblasts. This interaction is particularly relevant in breast-conserving surgeries, wherein the reciprocal

[1]Department of Immunology, Faculty of Health Sciences, University of Manitoba, Winnipeg, MB R3E 0T5, Canada

[2]Research Institute of Oncology & Hematology, CancerCareManitoba, Winnipeg, MB R3E 0V9, Canada

[3]Department of Surgery, Section of Plastic Surgery, Faculty of Health Sciences, University of Manitoba, Winnipeg, MB R3A 1M5, Canada

[4]Department of Pathology, Faculty of Health Sciences, University of Manitoba, Winnipeg, MB R3E 3P5, Canada

[5]Department of Biochemistry and Medical Genetics, Faculty of Health Sciences, University of Manitoba, Winnipeg, MB R3E 0J9, Canada

[6]Department of Oncology, Faculty of Medicine and Dentistry, University of Alberta, Edmonton, AB T6G 2E1, Canada

[7]Department of Obstetrics and Gynecology, Faculty of Medicine and Dentistry, University of Alberta, Edmonton, AB T6G 2E1, Canada

[8]Lead Contact

*Correspondence: afshin.raouf@umanitoba.ca

https://doi.org/10.1016/j.isci.2019.07.034

communication between tumor cells and the normal-associated fibroblasts (NAFs) could result in locoregional tumor recurrence. Initially, it was thought that NAFs prevent the development of a hyperplastic phenotype in breast epithelial cells and that they need to acquire an activated fibroblast phenotype to support breast tumor growth and progression (Dumont et al., 2013; Sadlonova et al., 2005; Shekhar et al., 2001). However, accumulating data now suggest that NAFs, similarly to TAFs, could support tumor cell proliferation (Fleming et al., 2010; Hu et al., 2008, 2009). This is evidenced by the recent reports indicating that addition of normal fibroblasts to patient-derived xenografts (PDXs) (Eirew et al., 2015) or MDA-MB-231 (Chatterjee et al., 2018) BCCs enhances tumor growth and take rate. These observations suggest that NAFs and TAFs may share unknown but common mechanisms to support tumor cell proliferation. In particular, the role of fibroblasts as a major component of tumor niche in supporting ER^+ tumor cell proliferation remains unexplored due to the lack of protocols to maintain and expand primary human ER^+BCCs *in vivo* and *ex vivo*. Recently, it was reported that primary human and mouse BCCs can be maintained in culture as organoids (Jamieson et al., 2017; Sachs et al., 2018). These assays, however, use a bulk heterogeneous population of cells, which makes the study of different subset of cells found in the tumor microenvironment difficult.

To address this gap, we developed a robust protocol to create patient-derived organoid cultures from TAFs and cancer cells separately obtained from primary malignant ER^+ human breast tumors as well as from NAFs obtained from the normal breast tissues. Using these organoid cultures, we uncovered a pro-tumorigenic paracrine signaling mechanism common to both NAFs and TAFs. We demonstrate that the constitutively secreted CCL7 (C-C motif chemokine ligand), IL6, and IL8 from either NAFs or TAFs result in release of platelet-derived growth factor (PDGF)-BB from ER^+BCCs, but not the normal breast cells, and that the PDGF-BB then acts in a paracrine manner causing IL1β production from NAFs and TAFs alike. IL1β then acts as a pro-proliferative factor, enhancing proliferation of both ER^+ cancer cells and fibroblasts. Last, we show that tamoxifen (Tam) is significantly more effective as first-line therapy for malignant ER^+ breast tumors if combined with IL1β and PDGF-BB receptor blockers.

RESULTS

NAF-Secreted Factors Enhance Primary ER^+ Breast Cancer Cell Proliferation in Organoid Cultures

To investigate the nature of interaction between NAFs and ER^+BCCs, we developed a 3-dimensional (3D) organoid model system initiated with primary malignant human ER^+ breast cancer cells (ER^+BCCs) and either stromal fibroblast obtained from the matching original tumors or breast reduction samples for up to 10 days (Figure 1A). In these cultures, ER^+BCCs (the $EpCAM^+$ cells) maintained their low expression of basal cell markers (CK5, CK14, αSMA, and p63) but high expression of luminal cell markers (EpCAM, MUC1, CK8+18, and ERα, Figure S1A). Likewise, NAFs and TAFs maintained the expression of fibroblast markers (CD73, CD90, CD105, CD13, and FSP1, Figure S1B). Moreover, these organoid cultures allowed the maintenance of ER^+BCCs and NAFs for up to 10 days, and for some samples increase in cell numbers was observed, although the data were variable (Figures S1C and S1D). These data suggest that our organoid culture provides a suitable *in vivo*-like environment to study the interaction between ER^+BCCs and fibroblasts. We therefore used this organoid culture system to assess NAFs' influence on ER^+BCC proliferation and found that only organoid cultures containing NAFs and ER^+BCCs showed significant increase in ER^+BCC numbers (1.97 ± 0.2-fold compared with 1.07 ± 0.24-fold, Figure 1B). Interestingly, fibroblast numbers were also increased in these organoid cultures containing NAFs and ER^+BCCs (2.2 ± 0.08-fold compared with 1.5 ± 0.02-fold, Figure 1C). As another source of primary NAFs we used fibroblasts obtained from tumor-free breast tissue contralateral to tumor-containing breast tissue (CNTB-Fs) and obtained similar results as NAFs (Figures 1B and 1C). As well, similar data were observed in 2D co-cultures of MCF7 and T47D cells with NAFs or CNTB-Fs (Figures S1E–S1G). Together, these data indicate that reciprocal interaction between the normal fibroblasts and cancer cells can induce proliferation of the ER^+BCCs.

To identify whether NAF-dependent proliferation of ER^+BCCs is mediated by secreted factors, ER^+BCCs were placed in organoid cultures for 2 days and subsequently growth medium was replaced with conditioned media (CM) obtained from NAF-ER^+BCC organoid co-cultures or organoid cultures containing each cell type separately for an additional 8 days when BCC ($EpCAM^+$) and NAF ($EpCAM^-$) cell numbers were analyzed (Figures 1D and 1E). Interestingly, only CM from the NAF-ER^+BCC organoid co-cultures

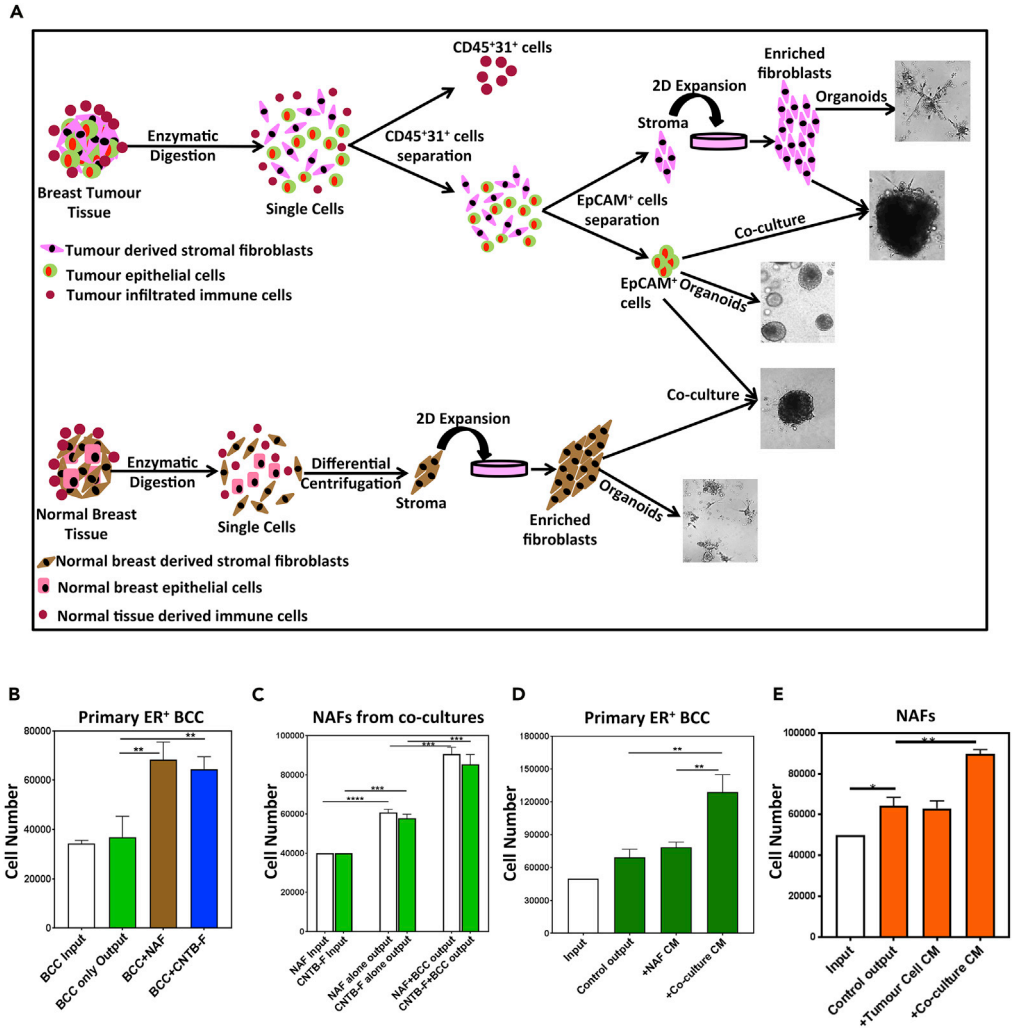

Figure 1. Normal Breast Fibroblasts Induce Proliferation of Primary ER+ Breast Cancer Cells in Organoid Cultures

(A) Experimental outline of organoid co-culture system to study stromal-epithelial interactions in primary tumors.

(B–E) (B) Organoid co-cultures were initiated with EpCAM+ primary human estrogen receptor-positive (ER+) breast cancer cells (BCCs) and normal breast fibroblasts obtained from either mammoplasty tissue (NAF) or matching contralateral non-tumor breast tissue (CNTB-F). Viable EpCAM+ BCC (B) or the EpCAM− fibroblast (C) cell numbers were quantified by flow cytometry at the beginning of the cultures (input) and after 10 days (output). EpCAM+ BCC (D) or the EpCAM− NAF (E) were placed in organoid cultures and treated with conditioned media (CM) collected from NAF and ER+BCC organoid co-cultures, and after 10 days total cell numbers were obtained via flow cytometry.

For all the experiments, average cell numbers and standard error of the mean (SEM) are based on primary ER+ breast cells obtained from three individual tumors and represented as bar graphs (**p < .005, ***p < .0005, and ****p < .00005).

significantly increased the proliferation of BCCs (2.58 ± 0.3-fold compared with 1.38 ± 0.14-fold) and NAFs (1.87 ± 0.2 fold-compared with 1.22 ± 0.08-fold) compared with the other CMs (Figures 1D and 1E). These data suggest that interaction of NAFs with ER+BCCs results in secretion of pro-proliferative factors, which are not present in the ER+BCCs or NAF-only cultures, and that these secreted factors are sufficient to enhance the proliferation of both cell types in these cultures without the requirement for cell-cell contact.

IL1β in NAF-BCC Co-culture CM Induces ER+BCCs Proliferation

Secreted cytokines and growth factors present in the CM collected from organoid cultures containing both NAF and ER+BCCs or single cultures of each cell type were analyzed using a cytokine ELISA array (Figure 2A

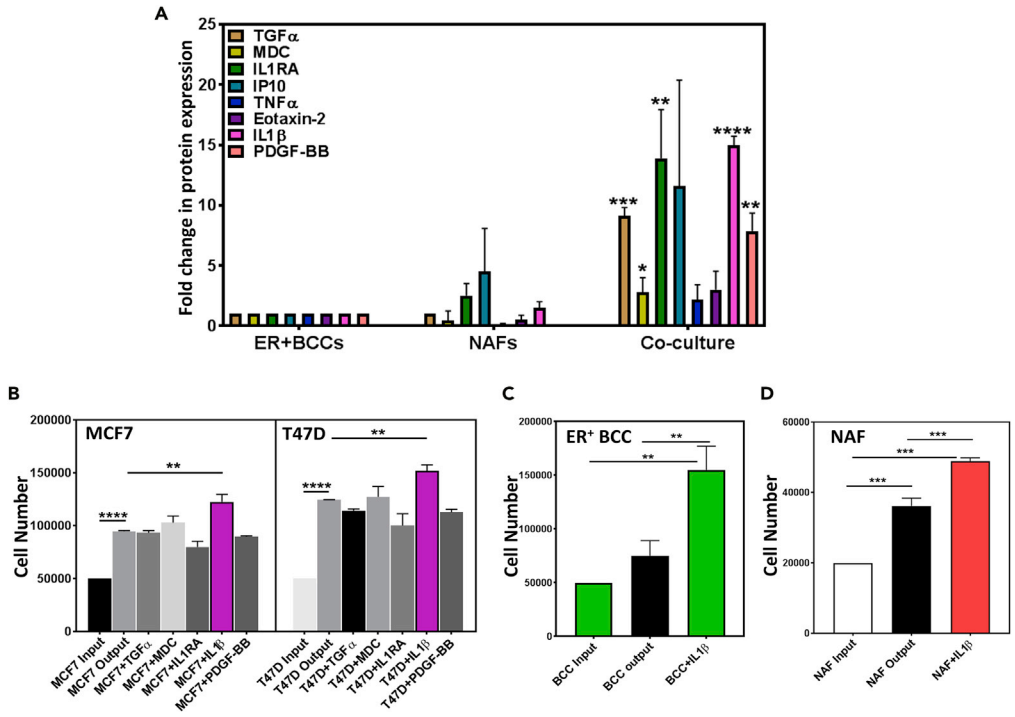

Figure 2. Co-culturing ER$^+$BCCs with NAFs Results in IL1β Secretion that Induces Proliferation of both Cell Types

(A) Cytokine ELISA array analysis of conditioned media (CM) obtained from organoid cultures consisting of EpCAM$^+$ ER$^+$BCC only, NAF only, or co-cultures of both cell types identified five cytokines to be significantly upregulated in the co-cultures (Table S2). Average from three biological replicates and standard error of the mean (SEM) are plotted as bar graphs where average cytokine levels in BCCs are set to 1.

(B) MCF7 and T47D cells were placed in organoid cultures and treated with different cytokines for 8 days, and average cell numbers and SEM from three independent experiments are depicted in the bar graphs.

(C and D) (C) ER$^+$BCCs and (D) NAFs were grown separately as organoids in the presence of recombinant IL1β (rIL1β) for 8 days.

Average cell numbers and SEM are based on primary ER$^+$ breast cells obtained from three individual tumors and plotted as bar graphs. (*p < .05, **p < .005, ***p < .0005, and ****p < .00005).

and Table S1). Eight cytokines were present at significantly higher levels in the CM of NAF-ER$^+$BCC co-cultures compared with the CM of NAF- or BCC-only cultures (Figure 2A). Of these eight, five cytokines (TGF-α, MDC, IL1RA, IL1β, and PDGF-BB) were selected for further examination based on their significant differential secretion (>3- to 5-fold). Interestingly, only recombinant IL1β (rIL1β) significantly increased the proliferation of MCF7 and T47D BCCs (Figure 2B) and the primary ER$^+$BCCs (Figure 2C), and NAFs (Figure 2D) grown in organoid cultures compared with the vehicle controls. Although rIL1β induced proliferation of both the cancer cells and fibroblasts, *IL1β* target genes were significantly upregulated in the NAFs (Figure S2A), but not in MCF7 (Figure S2B).

In contrast to the pro-proliferative effect of rIL1β on ER$^+$BCCs and NAFs, rIL1β showed an antiproliferative effect on normal breast epithelial progenitor cells. Recombinant IL1β significantly impaired acinar structure formation by normal breast epithelial cells in Matrigel (Figure S2C), decreased CD49f and EpCAM progenitor marker expression (2.1 ± 0.3-fold and 1.64 ± 0.2-fold respectively, Figure S2D), decreased total cell number in Matrigel (3.33 ± 0.64-fold, Figure S2E), and significantly decreased the progenitor cell proliferation (1.73 ± 0.25-fold, Figure S2F).

IL1β Is Secreted by Fibroblasts and Not the Breast Cancer Cells in NAF-BCC Co-cultures

To understand the source of IL1β in the organoid cultures, we examined IL1β expression in the co-cultures of ER$^+$ MCF7 and T47D cells with NAFs. MCF7, T47D, and NAFs express very low levels of *IL1β* transcripts and protein compared with the triple-negative MBA-MD-231 cells (Figures 3A and 3B). To ascertain the

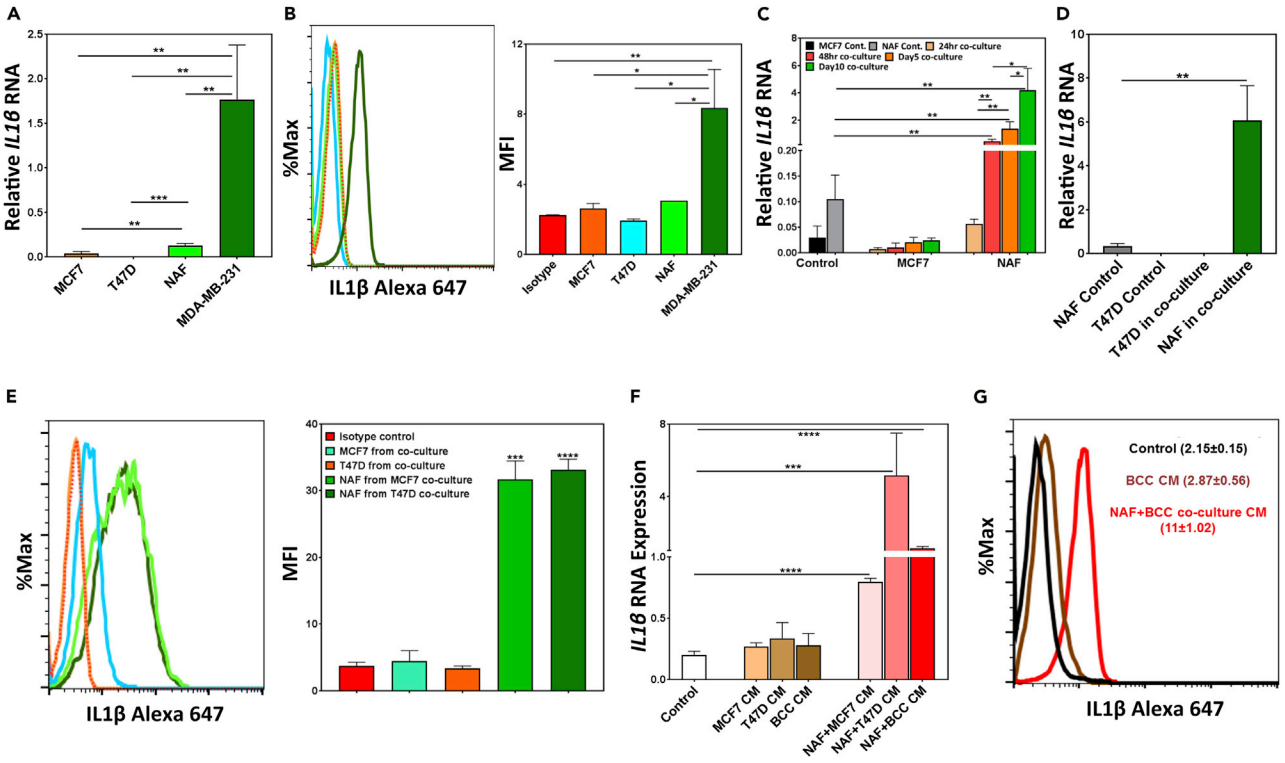

Figure 3. Fibroblasts Produce IL1β in Organoid Co-cultures with ER$^+$ Breast Cancer Cells

(A–D) *IL1β* transcripts (A) and protein (B) levels were measured in MCF7, T47D, NAFs, and MDA-MB-231 cells by qPCR and intracellular flow cytometry. NAFs were co-cultured with MCF7 (C) and T47D (D) cells and after respective days, breast cancer cells (EpCAM$^+$) and NAFs (EpCAM$^-$) were separated by flow cytometry and *IL1β* transcript expression was obtained by qPCR.

(E) IL1β protein expression was measured in NAFs co-cultured with MCF7 and T47D by intracellular flow cytometry.

(F) NAFs were treated with conditioned media (CM) obtained from either breast cancer cell (MCF7, T47D, and primary ER$^+$BCC)-only cultures or from NAFs and breast cancer cells in co-cultures for 6 h, and *IL1β* transcript expression was measured by qPCR.

(G) IL1β protein expression was measured in NAFs by intracellular flow cytometry following treatment with CM from ER$^+$BCC-only cultures or NAF and ER$^+$BCC co-cultures.

All the data are represented as either bar graphs or bold text with mean ± SEM and are based on primary ER$^+$ breast cells obtained from three individual tumors (*p < .05, **p < .005, ***p < .0005, and ****p < .00005).

contribution of each cell type in IL1β production, MCF7 and T47D cells were placed in 2D adherent co-cultures with NAFs for up to 10 days. The EpCAM$^+$ MCF7 and T47D cells were separated from the EpCAM$^-$ NAFs in these co-cultures using flow cytometry and *IL1β* transcripts, and protein levels were quantified. In co-cultures, high levels of *IL1β* transcripts and proteins were detected only in the NAFs, but not in the BCCs (Figures 3C–3E), suggesting that the presence of ER$^+$BCCs induces IL1β production in NAFs. To assess if secreted factors are responsible for the BCC-induced IL1β secretion from fibroblasts, NAFs were treated with CM obtained from cultures initiated with MCF7, T47D, or primary ER$^+$BCCs only or in co-culture with NAFs, and *IL1β* transcript levels and protein expressions were examined. Interestingly, only the CM from the co-cultures, but not the BCC-only cultures, was able to induce *IL1β* transcript (after 6-h exposure to CM) and protein levels in NAFs (Figures 3F and 3G). This is in keeping with our observation that rIL1β enhanced *IL1β*-target genes' expression after 6 h (Figure S2A).

To examine, whether different sources of fibroblasts can also secrete IL1β in co-cultures through similar mechanisms, MCF7 and T47D cells were placed in co-cultures with fibroblasts obtained from primary ER$^+$ human breast tumor adjacent tissue (TAT-Fs), CNTB-Fs, and NAFs. Fibroblasts isolated from different sources showed low *IL1β* transcript levels as in NAFs (Figure S3A). However, when placed in co-cultures with BCCs (Figure S3B) or exposed to the CM from these co-cultures (Figure S3C), *IL1β* transcript expression was significantly increased in all fibroblasts regardless of their origin. Interestingly, TAT-Fs showed much higher expression of *IL1β* transcripts and induced proliferation of T47D cells when placed in co-cultures or exposed to CM from T47D co-cultures compared with NAFs and CNTB-Fs (Figures S3B–S3E).

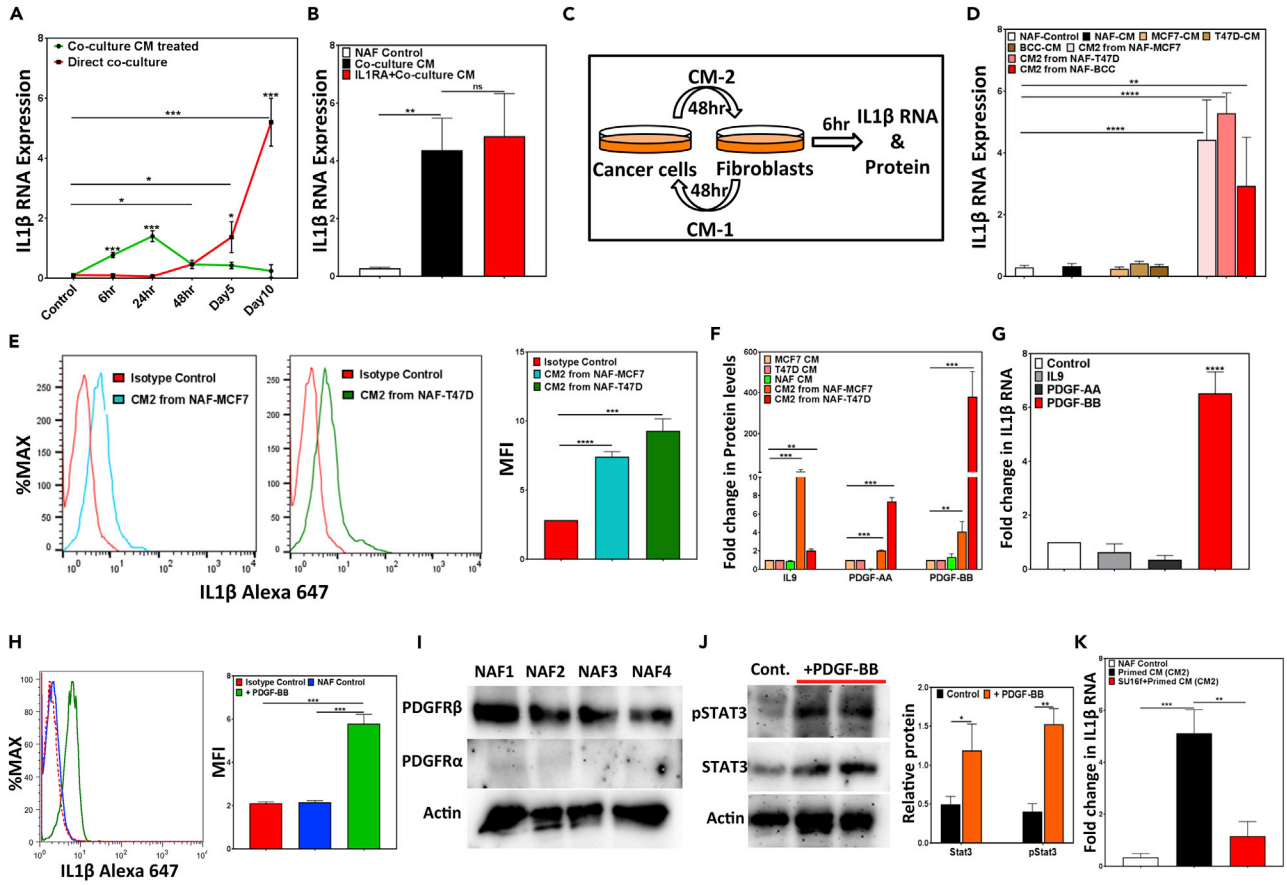

Figure 4. ER$^+$BCC-Induced IL1β Production from Fibroblasts Requires Secreted Factors from Fibroblasts

(A) *IL1β* transcript levels were quantified in NAFs either in co-cultures with MCF7 or treated with co-cultured conditioned media (CM) for up to 10 days.

(B) NAFs were treated with either IL1RA or vehicle controls for 48 h and then with NAF and MCF7 co-culture CM for 6 h and *IL1β* transcript level was measured.

(C) Experimental outline of 2D cultures for (D–F).

(D) *IL1β* transcript expression was measured in NAFs following treatment with CM1 and CM2 for 6 h.

(E) IL1β protein expression was measured in NAFs by intracellular flow cytometry following exposure to CM2 for 48 h.

(F) Cytokine ELISA array was used to compare cytokine levels in CMs from NAFs, MCF7, T47D, and CM2 (also Table S2). Cytokine expression is represented as fold changes.

(G) *IL1β* transcript levels were quantified in NAFs following 6 h treatment with recombinant IL9, PDGF-AA, and PDGF-BB.

(H) IL1β protein levels were quantified in NAFs following 48 h treatment with recombinant PDGF-BB.

(I) Representative western blots showing PDGFRα and PDGFRβ expressions in four different NAF samples.

(J) Representative western blot showing total STAT3 and phospho-STAT3 protein expression in NAFs treated with PDGF-BB. Average pSTAT3 expression is normalized to total STAT3 expression and shown as bar graphs.

(K) IL1β transcript expression was measured in NAFs following treatment with CM2 for 6 h with or without 48-h pre-incubation with SU16f.

All data are represented as bar graphs with mean ± SEM from three independent experiments (*p < .05, **p < .005, ***p < .0005, and ****p < .00005).

Fibroblast-Induced PDGF-BB Secretion by Breast Cancer Cells Causes IL1β Secretion from Fibroblasts

To understand the dynamics of IL1β production by NAFs, we examined *IL1β* transcript levels in NAFs either in co-culture with BCCs (MCF7) or treated with co-culture CM for up to 10 days. Interestingly *IL1β* transcript levels in NAFs treated with co-culture CM increased as early as 6 h (6.99 ± 1.7-fold) and continued to increase up to 24 h (12.5 ± 1.5-fold), but sharply declined thereafter (Figure 4A). In the co-cultures, however, *IL1β* transcript levels in NAFs significantly increased only after 48 h and continued to rise thereafter (Figure 4A). As MCF7, T47D, and NAFs express IL1β receptor IL1R1 ubiquitously (Figure S4A), it is possible that IL1β expression is regulated through a feedforward mechanism. However, blocking IL1β receptor IL1R1 with a receptor antagonist (IL1RA) could not prevent the co-culture CM-induced *IL1β* transcript

increase in NAFs (Figure 4B), suggesting that secreted factors other than IL1β are responsible for increased IL1β production in NAFs. To separately assess the contribution of secreted factors from the NAFs and the BCCs to the elevated IL1β levels, MCF7, T47D, or primary ER$^+$BCCs were exposed to CM obtained from NAF-only cultures for 48 h to obtain "primed-CM" (CM2, Figure 4C) and *IL1β* transcript levels were examined in NAFs exposed to the primed-CM for 6 h (Figure 4D). As controls, NAFs were also exposed to CM from MCF7, T47D, or primary ER$^+$BCCs-only cultures. Interestingly, only primed-CM significantly increased *IL1β* transcripts and protein levels in NAFs (Figures 4D and 4E), suggesting that secreted factors from both NAFs and BCCs are required to cause IL1β production from NAFs.

To identify secreted cytokines and growth factors involved in the crosstalk between NAFs and BCCs, CM obtained from NAF, MCF7, and T47D as well as the "primed-CM" (CM2) were analyzed using cytokine ELISA arrays. Three cytokines (IL9, PDGF-AA, and PDGF-BB) were identified to be significantly elevated in CM2 compared with the NAF- or BCC-only CMs (Figure 4F) of which, only recombinant PDGF-BB induced *IL1β* transcript (6.5 $\pm$ 0.79 fold) and protein (2.68 $\pm$ 0.11 fold) expression in NAFs after 6 and 48 h, respectively (Figures 4G and 4H, Table S2). It is noteworthy that NAF-T47D co-culture CM contained the highest PGDF-BB level (Figure 4F). Mechanistically, PDGF-BB signaling is conducted through interaction with its cognate cell surface receptors and activation of *STAT* signaling. Interestingly, NAFs show strong expression for the β- but not the α-form of the PDGF-BB receptor (Figure 4I) and that PDGF-BB activates *STAT3* signaling in these cells (Figure 4J). Moreover, activation of PDGF receptors is required for primed-CM-induced IL1β production from NAFs (Figure 4K), because the response was eliminated by pre-incubation with the selective PDGF-BB receptor inhibitor SU16f. In contrast to ER$^+$BCCs, the IL1β and PDGF-BB levels did not increase in 3D co-cultures of normal EpCAM+ primary breast epithelial cells and NAFs (Figures S4B–S4D). Also, EpCAM+ primary breast epithelial cells treated with recombinant PDGF-BB for 6 h did not increase IL1β transcript expression in them (Figure S4E). However, similar to IL1β, recombinant PDGF-BB also induced proliferation of NAFs in cultures (Figures S4F–S4H).

Constitutively Secreted Cytokines from NAFs Induce PDGF-BB Secretion from Breast Cancer Cells

To further explore the paracrine mechanisms involved in PDGF-BB production from BCCs, we compared the NAF-CM with the MCF7- and T47D-CM and identified four cytokines (CCL7, IL6, IL8, and GROα) that were uniquely secreted by NAFs (Figure 5A and Table S2). Interestingly, IL6 and IL8 together, but not alone, as well as CCL7 stimulated (2.6 $\pm$ 0.6-fold and 6.6 $\pm$ 1.5-fold, respectively) *PDGFB* gene expression in the primary ER$^+$BCCs; however, CCL7 is the major inducer of PDGF-BB production by ER$^+$BCCs (Figures 5B and 5C). GROα had no effect on PDGF-BB production. We found that IL6, IL8, and CCL7 are expressed at significant levels in the normal breast, ER$^+$ breast tumors, and the matching tumor-adjacent breast tissue (Figure 5D). These data suggest that the secretion of these cytokines does not require the presence of ER$^+$BCCs. However, the tumor microenvironment consists of activated TAFs that do not show sustained IL1β secretion (Figure 6A), suggesting that TAFs require the presence of ER$^+$BCCs to maintain IL1β secretion (Figure 6B). Interestingly however, TAFs induced MCF7 and T47D proliferation more significantly than NAFs in co-cultures (Figures S5A and S5B). To this end we found that similar to NAFs TAF-CM induces PDGF-BB secretion in MCF7 and T47D cells, which in turn causes IL1β production from TAFs (Figures 6C–6F and S5A–S5F).

TAFs and Infiltrating Immune Cells Create an IL1β-Enriched Microenvironment in ER$^+$ Breast Tumors

Our data describe a paracrine signaling mechanism between ER$^+$BCCs, NAFs, and TAFs that result in the secretion of IL1β from fibroblasts without requirement for immune cell response, leading to tumor cell proliferation (Figure 6G). As predicted by our model, PDGF-BB and IL1β can only be detected in the tumor tissue, indicating that the cross talk between the TAFs and the ER$^+$BCCs and not the normal breast epithelial cells results in PDGF-BB and IL1β production (Figure 6H). Next, we examined if *PDGFB* and *IL1β* expression are predictive of primary ER$^+$ breast cancer prognosis using SurvExpress online database. Interestingly, *IL1β* and *PDGFB* expression significantly separated the high-risk group from the low-risk group (concordance index = 54.9, log rank equal curves p = 0.0052, risk group hazard ratio = 1.6 [confidence interval 1.15–2.27]) and that both *IL1β* and *PDGFB* were more significantly expressed in the high-risk group compared with the low-risk group (Figures S5G and S5H). These observations suggest that the paracrine signaling described here could take place in the tumor environment and has clinical relevance to tumor progression. To further explore this possibility, we created the tumor microenvironment in NSG (NOD-scid

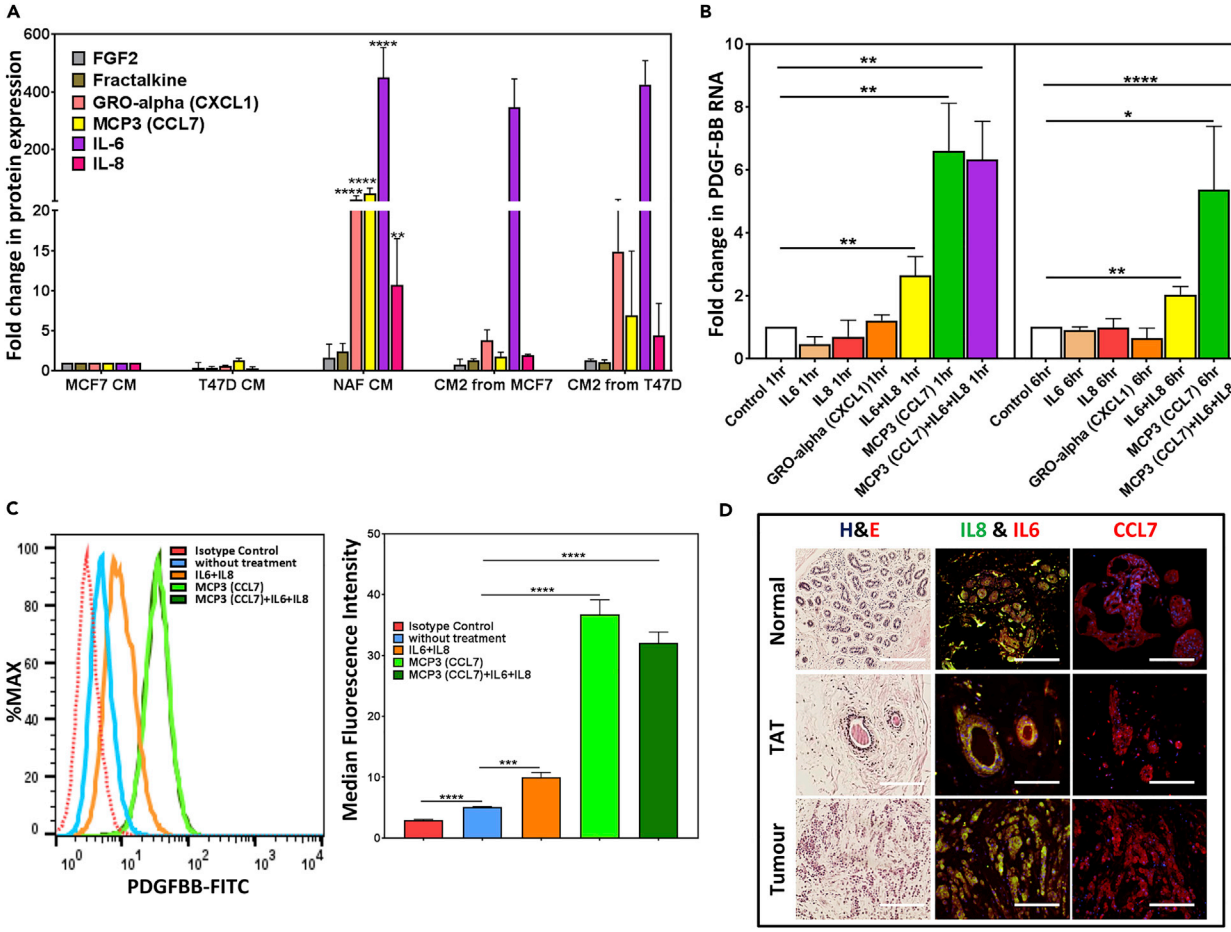

Figure 5. NAF-Secreted CCL7, IL6, and IL8 Induce PDGF-BB Production from Primary ER$^+$BCCs

(A) Cytokine array data (Figure 4F) identified CCL7, IL6, IL8, and GROα as cytokines highly secreted by only NAFs, but not by the MCF7 and T47D cells.

(B) *PDGFB* transcript levels were quantified via qPCR in EpCAM$^+$ primary ER$^+$BCC after 1- and 6-h treatment with recombinant IL6, IL8, CCL7, and GROα either alone or in combination.

(C) PDGF-BB protein expression in primary ER$^+$BCCs was quantified after 48-h treatment with recombinant CCL7, IL6, and IL8. All data are represented as bar graphs with mean ± SEM from three independent experiments (*p < .05, **p < .005, ***p < .0005, and ****p < .00005).

(D) Representative H&E and immunofluorescent images from three independent experiments showing IL6, IL8, and CCL7 protein expression in ER$^+$ breast tumor, matched tumor-adjacent, and healthy normal breast tissue sections. Scale bars, 200 μm.

IL2Rgamma^{null}) mice using TAFs and the ER$^+$ MCF7 BCCs and examined the impact of blocking IL1β (Anakinra) and PDGF (SU16f) signaling on tumor growth *in vivo*. We observed that xenografts generated in mice treated with Anakinra alone or with combination of Anakinra and SU16f showed statistically significant but modestly decreased tumor cell density compared with the xenografts obtained from untreated control mice (Figures 6I and S5I). SU16f-treated xenografts did not show any significant increase in necrotic or cell-free areas when compared with the untreated control xenografts. Notably, the intra-nipple injection model used allowed for confined growth within the mammary ducts. Accordingly, no difference in tumor weight was observed among the different treatment groups; hence alterations in tumor histology were not due to dramatic differences in tumor volume (data not shown).

In the tumor microenvironment, however, in addition to TAFs (Figure S6A), the tumor-infiltrating immune cells and the vascular endothelial cells also contribute to tumor cell proliferation. To examine the contribution of the immune and blood vessel cells to tumor cell proliferation, we utilized the cytokine ELISA array platform to analyze the secreted cytokine profile of CD45$^+$CD31$^+$ cells obtained from three primary ER$^+$ breast tumor samples after 10 days in 3D organoid culture (Figures 7A, S6B, and S6C). The analysis identified that some of the same cytokines secreted by the NAF and ER$^+$BCC co-cultures were also secreted

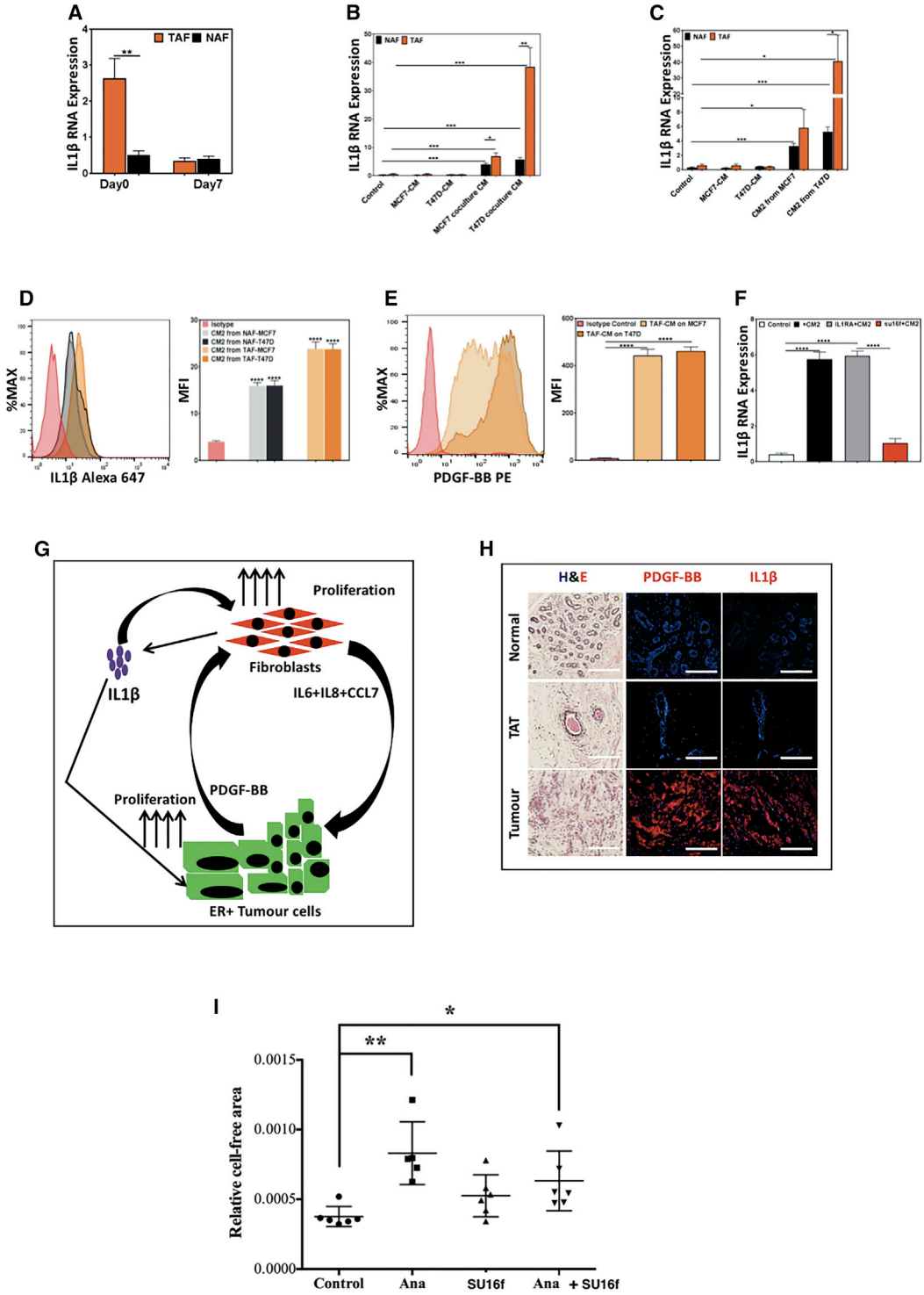

Figure 6. Crosstalk between TAFs and ER$^+$BCCs Results in IL1β Production by TAFs

(A) *IL1β* transcript expression was measured in TAFs and NAFs immediately after isolation (day 0) and after 7 days of 2-dimensional (2D) adherent cultures.

(B) NAFs and TAFs were treated with conditioned media (CM) from MCF7- and T47D-only cultures or from the 2D co-culture with NAFs or TAFs for 6 h, and *IL1β* transcript levels in the fibroblasts were quantified via qPCR.

(C) NAFs and TAFs were treated with CMs from MCF7 and T47D or (CM2, from Figure 4C) for 6 h, and *IL1β* transcript levels were measured.

Figure 6. *Continued*

(D) IL1β protein expression was measured in NAFs and TAFs following treatment with CM2 for 48 h by intracellular flow cytometry.

(E) PDGF-BB protein expression was measured in MCF7 and T47D following treatment with CM from TAFs for 48 h by intracellular flow cytometry.

(F) *IL1β* transcript expression was measured in TAFs following treatment with CM2 for 6 h with or without 48-h pre-incubation with IL1RA or SU16f. All data are represented as bar graphs with mean ± SEM from three independent experiments.

(G) Graphical summary of the crosstalk between fibroblasts and breast cancer cells resulting in IL1β secretion from the fibroblasts.

(H) Representative H&E-stained sections and immunofluorescent images showing PDGF-BB and IL1β protein expression from three individual ER^+ breast cancer tumors, matched tumor-adjacent, and three healthy normal breast tissues.

(I) Tumor progression was monitored in an orthotopic mouse breast cancer model using TAFs and MCF7 cells. Mice were either treated with Anakinra (Ana), SU16f (Su), Ana + Su, or vehicle control. Cell-free areas of H&E sections from each tumor was obtained (Figure S5I), normalized to the total area for each xenograft section, and plotted in dot plots. Scale bars, 200 μm. *p < .05, **p < .005, ***p < .0005, and ****p < .00005.

at significantly higher levels (Table S3) by the tumor-associated $CD45^+31^+$ cells. Compared with the ER^+BCC-NAF organoid co-cultures, the tumor-associated $CD45^+CD31^+$ cells secrete 5.7 ± 0.48-fold more IL1β, 1.5 ± 2-fold CCL7, 1.2 ± 0.2-fold IL6, and 1.1 ± 0.02-fold IL8 (Figure 7A and Table S3). The immunophenotyping analysis of the tumor-associated $CD45^+31^+$ cells revealed a higher presence of T cells and lower but detectable levels of monocytes, B cells, and natural killer cells (Figure S6D), which matched the secreted cytokine profile of these cells (Figure S6E).

Disrupting the ER^+BCC-TAF Paracrine Signaling Significantly Amplifies Tamoxifen Efficacy

Our data indicate that the paracrine signaling between the ER^+BCC and fibroblasts cooperates with the $CD45^+CD31^+$ cells in the tumor microenvironment to create an IL1β-enriched niche that augments tumor cell proliferation. We therefore examined if the disruption of IL1β production and signaling in the tumor microenvironment would augment the cytostatic effect of Tam on the ER^+BCCs. For this purpose, we reconstructed the tumor microenvironment in organoid cultures using the primary ER^+BCCs, TAFs, and $CD45^+CD31^+$ cells separately obtained from the same original tumor (Figure 7B). Tumor-associated $CD45^+CD31^+$ cells showed a small (20%–30%) decrease in cell number in these organoid cultures over 10 days (Figure S6B). We examined the effective dose of Tam through its ability to decrease MCF7 cell proliferation in organoid cultures (Figure S6F) and found that 100 nM Tam was ineffective in reducing MCF7 cell proliferation, whereas 1 μM Tam significantly reduced proliferation of these, and we therefore chose these concentrations for our experiments. To examine the contribution of the TAFs and $CD45^+CD31^+$ cells to tumor cell proliferation, we quantified $AnnexinV^-EpCAM^+$ cell numbers in organoid cultures initiated with primary ER^+BCCs alone or in co-cultures with TAFs, $CD45^+CD31^+$, or all three cell types together. ER^+BCCs expanded 1.3 ± 0.1-fold in the organoid cultures. However, ER^+BCCs showed further proliferation in co-cultures with TAFs (1.96 ± 0.3) and $CD45^+CD31^+$ (1.72 ± 0.2), but no additional proliferation was detected in co-cultures consisting of all three cell types (Figures 7C–7F). In contrast to MCF7 cells (Figure S6E), 100 nM Tam prevented the expansion of ER^+BCCs in all the cultures. A selective PDGF-BB receptor inhibitor SU16f and an IL1R1 antagonist IL1RA, showed similar effects as Tam in all the co-cultures, although the results were variable. However, the ER^+BCC proliferation in co-cultures were significantly curtailed when organoids were treated with Tam, SU16f, and IL1RA, suggesting that these blockers work synergistically with Tam. In TAF-ER^+BCC organoid co-cultures, SU16f and IL1RA were as effective as Tam in decreasing ER^+BCC proliferation.

DISCUSSION

In this report, we describe a fibroblast-initiated paracrine signaling mechanism that enhances ER^+BCC proliferation. We show that cytokines constitutively secreted by NAFs and TAFs alike (CCL7 and/or IL6 and IL8) result in increased expression and secretion of PDGF-BB from primary ER^+BCCs but not the normal breast epithelial cells. In this regard, CCL7 makes the most significant contribution toward the release of PDGF-BB from ER^+BCCs. CCL7 is a ligand for CCR1–3 receptors, among which expression of CCR3 has recently been shown to be associated with luminal-type breast cancers (Gong et al., 2016). Also, the interaction between CCL7 and CCR3 has been shown to promote colon cancer cell metastasis via ERK-JNK signaling (Lee et al., 2016). The role of IL6 and IL8 in breast cancer progression has been well studied in that both cytokines increase the invasiveness and the metastatic potential of ER^+ and ER^- breast cancers

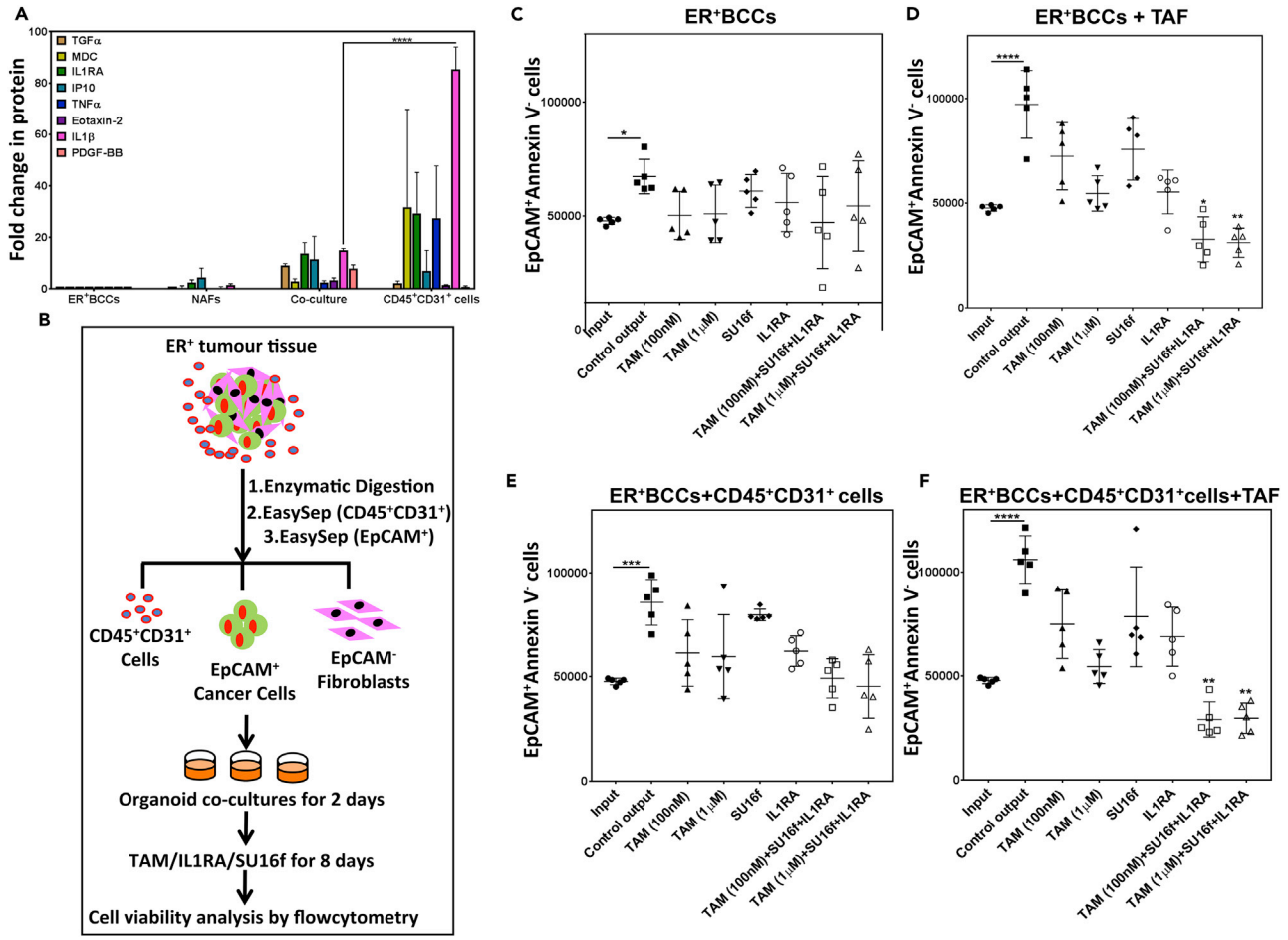

Figure 7. Deconstruction and Reconstruction of Tumor Microenvironment

(A) Cytokine ELISA array was used to examine cytokines present in the CM obtained from organoid cultures of primary ER$^+$BCCs, matched tumor-associated CD45$^+$CD31$^+$ cells, NAFs, and NAFs-ER$^+$BCCs co-cultures. Cytokines that were secreted at high concentration by the NAF-ER$^+$BCCs co-cultures, as well by the CD45$^+$CD31$^+$ cells, are shown (Table S3). Average from three biological replicates and SEM are plotted as bar graphs where average cytokine levels in breast cancer cells are set to 1.

(B–F) (B) Experimental outline for (C–F). The ER$^+$BCCs (C), ER$^+$BCCs with BCC-associated fibroblasts (TAFs) (D), ER$^+$BCCs with matching BCC-associated CD45$^+$CD31$^+$ cells (E), and all three cell types together (F) were put into organoid cultures for 2 days and then treated with IL1RA, SU16F, and tamoxifen (Tam) as indicated for additional 8 days, and the number of viable (AnnexinV$^-$) EpCAM$^+$BCCs was determined by flow cytometry. The data represented as dot plots from primary ER$^+$ breast cells obtained from five individual tumors, and average cell numbers and SEM are plotted (*$p < .05$, **$p < .005$, ***$p < .0005$, and ****$p < .00005$, statistical significance was tested against the input controls).

by activating signaling through their receptors, gp130 and CXCR1 (Ginestier et al., 2010; Iliopoulos et al., 2010; Korkaya et al., 2011; Sasser et al., 2007; Sheridan et al., 2006; Studebaker et al., 2008). Previous reports indicate that PDGF-BB increases the expression of IL6 and IL8 in different cell types (van Steensel et al., 2010). Here we show that increased PDGF-BB levels increases in ER$^+$BCCs due to CCL7, IL6, or IL8 cytokine signaling. IL6, IL8, and CCL7 presumably increase PDGF-BB expression by activating their cognate receptors, which have been previously shown to be expressed in ER$^+$BCCs. The PDGF-BB secreted from ER$^+$BCC signals through its receptor PDGFRβ to induce IL1β production in the normal and activated fibroblasts without the requirement for IL1β receptor IL1R1 activation, suggesting that fibroblast secretion of IL1β is not regulated through a feedforward mechanism. Signaling through the PDGFRβ activates the STAT3 and ERK signaling, which have previously been reported (O'Brien et al., 1999; Tian et al., 2017) to induce IL1β transcripts and protein levels. These signaling pathways therefore are the most likely mechanism of PDGF-BB-induced IL1β production from NAFs and TAFs. We also show that although IL1β suppresses the proliferation of normal breast epithelial progenitors, it creates a pro-oncogenic environment by

activating proliferation signals in ER$^+$BCCs. Therefore, our data suggest that features distinguishing the ER$^+$BCCs from the normal breast epithelial cells are the ability to take advantage of fibroblast-secreted factors to produce PDGF-BB and to utilize IL1β signaling as a pro-proliferative signal. Our orthotopic mouse tumor data suggest that blocking IL1β could potentially decrease tumor volume in xenografts initiated with TAFs and BCCs; however, additional data are required to provide stronger support for this observation.

Our findings suggest that in patients with breast cancer undergoing breast-conserving surgeries, any residual BCCs could take advantage of cytokines constitutively secreted by the fibroblasts and initiate the paracrine signaling cascade described here to transform the normal breast tissue niche into an IL1β-enriched niche that supports their proliferation. Previously it was demonstrated that NAFs are able to support cancer cell proliferation *in vivo*; however, they do so at much lower efficiency than TAFs (Chatterjee et al., 2018; Olumi et al., 1999). It is therefore inviting to hypothesize that in normal breast tissue, epigenetic or accumulating mutational events could enable the normal epithelial cells to utilize the CCL7 or IL6 and IL8 signaling pathways to produce PDGF-BB, ultimately inducing IL1β release from fibroblasts. However, the ability to produce PDGF-BB in the presence of these cytokines, on its own, is not sufficient to promote the proliferation of breast epithelial cells because we show that IL1β significantly diminishes the proliferation of normal breast epithelial progenitors.

Using cytokine array platform, we found that in the tumor microenvironment the immune cells, in particular monocytes/macrophages, are the most significant sources of IL1β when compared with fibroblasts. We therefore have demonstrated the clinical significance of our findings by assessing the individual contributions of TAFs and immune cells in tumor response to endocrine therapy. By reconstructing the tumor microenvironment using ER$^+$BCCs, TAFs, and the immune cells from the same primary tumors, we demonstrate that the effectiveness of endocrine therapy (Tam) can be significantly augmented in the presence of IL1R1 and PDGFRβ blockers. This observation is particularly interesting because examining the contribution of tumor-infiltrating leukocytes (TILs) to ER$^+$BCC proliferation and response to endocrine therapy cannot be examined through the other available models to study ER$^+$ tumor microenvironment. Although primary tumors can be expanded through several passages in immunodeficient mice (i.e., PDX), only 4%–6% of primary ER$^+$ tumors form xenografts. Moreover, it is unlikely that activated TILs would be propagated in passaged xenografts. On the other hand, the ER$^+$BCC lines (MCF7 and T47D) can readily form xenografts in immunodeficient mice. However, these cell lines have been generated from metastatic breast cancer tumors, which might not be an accurate representation of primary ER$^+$ breast cancer tumors. Also, owing to major histocompatibility complex molecule incompatibility, TILs cannot be included in these xenografts. Finally, our results suggest that patients diagnosed with malignant ER$^+$ breast cancer may benefit from combination therapy consisting of IL1R1 and PDGFRβ blockers to enhance the effectiveness of endocrine therapies such as Tam.

Limitations of the Study

In our study we provide evidence that regularly secreted cytokines from fibroblasts result in creation of an IL1β-enriched environment that supports ER$^+$BCC proliferation. Such paracrine signaling might be important to tumor progression and therapy response. However, there are limitations to our study due to some experimental constraints. The impact of blocking IL1β and PDGF-BB signaling on tumor growth *in vivo* was rather modest. However, the *in vivo* model we used did not ensure that fibroblasts and tumor cells will be confined to the xenografted site in the mammary gland. This issue could be addressed by using PDXs where tumor cells and fibroblasts are present in the primary breast tumor section. Moreover, the use of combination therapy that includes endocrine therapy along with IL1β and PDGF-BB signaling blockers might provide more definitive data with respect to decreased tumor cell density.

Second, in our patient-derived organoid cultures, we used CD45+ immune cells and the CD31+ vascular endothelial cells, which did not allow us to evaluate the contribution of each cell type to tumor cell growth and response to therapy separately. Owing to the low frequency at which these cells are present in primary breast tumors, obtaining each of these cell types separately in sufficient numbers proved difficult.

METHODS

All methods can be found in the accompanying Transparent Methods supplemental file.

SUPPLEMENTAL INFORMATION

Supplemental Information can be found online at https://doi.org/10.1016/j.isci.2019.07.034.

ACKNOWLEDGMENTS

This work was made possible by Postdoctoral Fellowships from Research Manitoba and the Canadian Breast Cancer Foundation- Prairie/NWT region to S.C., and operating grants from the Canadian Breast Cancer Foundation (CBCF) and University of Manitoba and CancerCareManitoba Foundation (CCMF) to A.R. L.C.M. acknowledges support from the Canadian Institutes of Health Research (CIHR), CBCF, and CCMF. A.J.M. acknowledges Research Manitoba for supporting CLL cluster and flow cytometry core. L.M.P. was supported by a Translational Health Chair in Cancer from Alberta Innovates. Also, we would also like to thank Christine Zhang and Xun Wu and Monroe Chan for help with flow cytometry experiments. This study was supported by the Manitoba Tumour Bank (MTB), Winnipeg, Manitoba, funded in part by CancerCare Manitoba Foundation (CCMF) and the Canadian Institutes of Health Research (CIHR). MTB is a member of the Canadian Tissue Repository Network.

AUTHOR CONTRIBUTIONS

S.C. conducted the experiments and co-wrote the manuscript and conceptualized the project. A.B. conducted some experiments. J.S. provided pathological evaluation of the tumor-adjacent breast tissue samples. E.B. contributed to data interpretation. A.J.M contributed to the immunophenotyping experiments of tumor-derived leukocytes. L.C.M provided critical review of the manuscript. J.L., G.Z., and L.-M.P. conducted the xenograft experiments. V.B. analyzed the xenograft data. A.R. helped with data analysis and co-wrote the manuscript.

DECLARATION OF INTERESTS

The authors declare no competing interests.

Received: July 6, 2018
Revised: March 16, 2019
Accepted: July 18, 2019
Published: September 27, 2019

REFERENCES

Acharyya, S., Oskarsson, T., Vanharanta, S., Malladi, S., Kim, J., Morris, P.G., Manova-Todorova, K., Leversha, M., Hogg, N., Seshan, V.E., et al. (2012). A CXCL1 paracrine network links cancer chemoresistance and metastasis. Cell *150*, 165–178.

Allaoui, R., Bergenfelz, C., Mohlin, S., Hagerling, C., Salari, K., Werb, Z., Anderson, R.L., Ethier, S.P., Jirstrom, K., Pahlman, S., et al. (2016). Cancer-associated fibroblast-secreted CXCL16 attracts monocytes to promote stroma activation in triple-negative breast cancers. Nat. Commun. *7*, 13050.

Bhowmick, N.A., Neilson, E.G., and Moses, H.L. (2004). Stromal fibroblasts in cancer initiation and progression. Nature *432*, 332–337.

Boimel, P.J., Smirnova, T., Zhou, Z.N., Wyckoff, J., Park, H., Coniglio, S.J., Qian, B.Z., Stanley, E.R., Cox, D., Pollard, J.W., et al. (2012). Contribution of CXCL12 secretion to invasion of breast cancer cells. Breast Cancer Res. *14*, R23.

Bussard, K.M., Mutkus, L., Stumpf, K., Gomez-Manzano, C., and Marini, F.C. (2016). Tumor-associated stromal cells as key contributors to the tumor microenvironment. Breast Cancer Res. *18*, 84.

Chatterjee, S., Basak, P., Buchel, E., Safneck, J., Murphy, L.C., Mowat, M., Kung, S.K., Eirew, P., Eaves, C.J., and Raouf, A. (2018). Breast cancers activate stromal fibroblast-induced suppression of progenitors in adjacent normal tissue. Stem Cell Reports *10*, 196–211.

Chatterjee, S., Laliberte, M., Blelloch, S., Ratanshi, I., Safneck, J., Buchel, E., and Raouf, A. (2015). Adipose-derived stromal vascular fraction differentially expands breast progenitors in tissue adjacent to tumors compared to healthy breast tissue. Plast. Reconstr. Surg. *136*, 414e–425e.

Cohen, N., Shani, O., Raz, Y., Sharon, Y., Hoffman, D., Abramovitz, L., and Erez, N. (2017). Fibroblasts drive an immunosuppressive and growth-promoting microenvironment in breast cancer via secretion of Chitinase 3-like 1. Oncogene *36*, 4457–4468.

Dumont, N., Liu, B., Defilippis, R.A., Chang, H., Rabban, J.T., Karnezis, A.N., Tjoe, J.A., Marx, J., Parvin, B., and Tlsty, T.D. (2013). Breast fibroblasts modulate early dissemination, tumorigenesis, and metastasis through alteration of extracellular matrix characteristics. Neoplasia *15*, 249–262.

Eirew, P., Steif, A., Khattra, J., Ha, G., Yap, D., Farahani, H., Gelmon, K., Chia, S., Mar, C., Wan, A., et al. (2015). Dynamics of genomic clones in breast cancer patient xenografts at single-cell resolution. Nature *518*, 422–426.

Erez, N., Truitt, M., Olson, P., Arron, S.T., and Hanahan, D. (2010). Cancer-associated fibroblasts are activated in incipient neoplasia to orchestrate tumor-promoting inflammation in an NF-kappaB-dependent manner. Cancer Cell *17*, 135–147.

Fleming, J.M., Miller, T.C., Quinones, M., Xiao, Z., Xu, X., Meyer, M.J., Ginsburg, E., Veenstra, T.D., and Vonderhaar, B.K. (2010). The normal breast microenvironment of premenopausal women differentially influences the behavior of breast cancer cells in vitro and in vivo. BMC Med. *8*, 27.

Gascard, P., and Tlsty, T.D. (2016). Carcinoma-associated fibroblasts: orchestrating the composition of malignancy. Genes Dev. *30*, 1002–1019.

Ginestier, C., Liu, S., Diebel, M.E., Korkaya, H., Luo, M., Brown, M., Wicinski, J., Cabaud, O., Charafe-Jauffret, E., Birnbaum, D., et al. (2010). CXCR1 blockade selectively targets human breast cancer stem cells in vitro and in xenografts. J. Clin. Invest. *120*, 485–497.

Gong, D.H., Fan, L., Chen, H.Y., Ding, K.F., and Yu, K.D. (2016). Intratumoral expression of CCR3

in breast cancer is associated with improved relapse-free survival in luminal-like disease. Oncotarget *7*, 28570–28578.

Guarnerio, J., Mendez, L.M., Asada, N., Menon, A.V., Fung, J., Berry, K., Frenette, P.S., Ito, K., and Pandolfi, P.P. (2018). A non-cell-autonomous role for Pml in the maintenance of leukemia from the niche. Nat. Commun. *9*, 66.

Hanahan, D., and Weinberg, R.A. (2011). Hallmarks of cancer: the next generation. Cell *144*, 646–674.

Hu, M., Yao, J., Carroll, D.K., Weremowicz, S., Chen, H., Carrasco, D., Richardson, A., Violette, S., Nikolskaya, T., Nikolsky, Y., et al. (2008). Regulation of in situ to invasive breast carcinoma transition. Cancer Cell *13*, 394–406.

Hu, M., Peluffo, G., Chen, H., Gelman, R., Schnitt, S., and Polyak, K. (2009). Role of COX-2 in epithelial-stromal cell interactions and progression of ductal carcinoma in situ of the breast. Proc. Natl. Acad. Sci. U S A *106*, 3372–3377.

Hugo, H.J., Lebret, S., Tomaskovic-Crook, E., Ahmed, N., Blick, T., Newgreen, D.F., Thompson, E.W., and Ackland, M.L. (2012). Contribution of fibroblast and mast cell (afferent) and tumor (efferent) IL-6 effects within the tumor microenvironment. Cancer Microenviron. *5*, 83–93.

Iliopoulos, D., Jaeger, S.A., Hirsch, H.A., Bulyk, M.L., and Struhl, K. (2010). STAT3 activation of miR-21 and miR-181b-1 via PTEN and CYLD are part of the epigenetic switch linking inflammation to cancer. Mol. Cell *39*, 493–506.

Jamieson, P.R., Dekkers, J.F., Rios, A.C., Fu, N.Y., Lindeman, G.J., and Visvader, J.E. (2017). Derivation of a robust mouse mammary organoid system for studying tissue dynamics. Development *144*, 1065–1071.

Karnoub, A.E., Dash, A.B., Vo, A.P., Sullivan, A., Brooks, M.W., Bell, G.W., Richardson, A.L., Polyak, K., Tubo, R., and Weinberg, R.A. (2007). Mesenchymal stem cells within tumour stroma promote breast cancer metastasis. Nature *449*, 557–563.

Korkaya, H., Liu, S., and Wicha, M.S. (2011). Breast cancer stem cells, cytokine networks, and the tumor microenvironment. J. Clin. Invest. *121*, 3804–3809.

Kuperwasser, C., Chavarria, T., Wu, M., Magrane, G., Gray, J.W., Carey, L., Richardson, A., and Weinberg, R.A. (2004). Reconstruction of functionally normal and malignant human breast tissues in mice. Proc. Natl. Acad. Sci. U S A *101*, 4966–4971.

Lee, Y.S., Kim, S.Y., Song, S.J., Hong, H.K., Lee, Y., Oh, B.Y., Lee, W.Y., and Cho, Y.B. (2016). Crosstalk between CCL7 and CCR3 promotes metastasis of colon cancer cells via ERK-JNK signaling pathways. Oncotarget *7*, 36842–36853.

Lu, H., Clauser, K.R., Tam, W.L., Frose, J., Ye, X., Eaton, E.N., Reinhardt, F., Donnenberg, V.S., Bhargava, R., Carr, S.A., et al. (2014). A breast cancer stem cell niche supported by juxtacrine signalling from monocytes and macrophages. Nat. Cell Biol. *16*, 1105–1117.

Makarem, M., Kannan, N., Nguyen, L.V., Knapp, D.J., Balani, S., Prater, M.D., Stingl, J., Raouf, A., Nemirovsky, O., Eirew, P., et al. (2013). Developmental changes in the in vitro activated regenerative activity of primitive mammary epithelial cells. PLoS Biol. *11*, e1001630.

O'Brien, C.A., Gubrij, I., Lin, S.C., Saylors, R.L., and Manolagas, S.C. (1999). STAT3 activation in stromal/osteoblastic cells is required for induction of the receptor activator of NF-kappaB ligand and stimulation of osteoclastogenesis by gp130-utilizing cytokines or interleukin-1 but not 1,25-dihydroxyvitamin D3 or parathyroid hormone. J. Biol. Chem. *274*, 19301–19308.

Olumi, A.F., Grossfeld, G.D., Hayward, S.W., Carroll, P.R., Tlsty, T.D., and Cunha, G.R. (1999). Carcinoma-associated fibroblasts direct tumor progression of initiated human prostatic epithelium. Cancer Res. *59*, 5002–5011.

Orimo, A., Gupta, P.B., Sgroi, D.C., Arenzana-Seisdedos, F., Delaunay, T., Naeem, R., Carey, V.J., Richardson, A.L., and Weinberg, R.A. (2005). Stromal fibroblasts present in invasive human breast carcinomas promote tumor growth and angiogenesis through elevated SDF-1/CXCL12 secretion. Cell *121*, 335–348.

Otomo, R., Otsubo, C., Matsushima-Hibiya, Y., Miyazaki, M., Tashiro, F., Ichikawa, H., Kohno, T., Ochiya, T., Yokota, J., Nakagama, H., et al. (2014). TSPAN12 is a critical factor for cancer-fibroblast cell contact-mediated cancer invasion. Proc. Natl. Acad. Sci. U S A *111*, 18691–18696.

Pickup, M., Novitskiy, S., and Moses, H.L. (2013). The roles of TGFbeta in the tumour microenvironment. Nat. Rev. Cancer *13*, 788–799.

Plaks, V., Kong, N., and Werb, Z. (2015). The cancer stem cell niche: how essential is the niche in regulating stemness of tumor cells? Cell Stem Cell *16*, 225–238.

Quail, D.F., and Joyce, J.A. (2013). Microenvironmental regulation of tumor progression and metastasis. Nat. Med. *19*, 1423–1437.

Sachs, N., de Ligt, J., Kopper, O., Gogola, E., Bounova, G., Weeber, F., Balgobind, A.V., Wind, K., Gracanin, A., Begthel, H., et al. (2018). A living biobank of breast cancer organoids captures disease heterogeneity. Cell *172*, 373–386.e10.

Sadlonova, A., Novak, Z., Johnson, M.R., Bowe, D.B., Gault, S.R., Page, G.P., Thottassery, J.V., Welch, D.R., and Frost, A.R. (2005). Breast fibroblasts modulate epithelial cell proliferation in three-dimensional in vitro co-culture. Breast Cancer Res. *7*, R46–R59.

Sasser, A.K., Sullivan, N.J., Studebaker, A.W., Hendey, L.F., Axel, A.E., and Hall, B.M. (2007). Interleukin-6 is a potent growth factor for ER-alpha-positive human breast cancer. FASEB J. *21*, 3763–3770.

Scherz-Shouval, R., Santagata, S., Mendillo, M.L., Sholl, L.M., Ben-Aharon, I., Beck, A.H., Dias-Santagata, D., Koeva, M., Stemmer, S.M., Whitesell, L., et al. (2014). The reprogramming of tumor stroma by HSF1 is a potent enabler of malignancy. Cell *158*, 564–578.

Sharon, Y., Raz, Y., Cohen, N., Ben-Shmuel, A., Schwartz, H., Geiger, T., and Erez, N. (2015). Tumor-derived osteopontin reprograms normal mammary fibroblasts to promote inflammation and tumor growth in breast cancer. Cancer Res. *75*, 963–973.

Shekhar, M.P., Werdell, J., Santner, S.J., Pauley, R.J., and Tait, L. (2001). Breast stroma plays a dominant regulatory role in breast epithelial growth and differentiation: implications for tumor development and progression. Cancer Res. *61*, 1320–1326.

Sheridan, C., Kishimoto, H., Fuchs, R.K., Mehrotra, S., Bhat-Nakshatri, P., Turner, C.H., Goulet, R., Jr., Badve, S., and Nakshatri, H. (2006). CD44+/CD24- breast cancer cells exhibit enhanced invasive properties: an early step necessary for metastasis. Breast Cancer Res. *8*, R59.

Studebaker, A.W., Storci, G., Werbeck, J.L., Sansone, P., Sasser, A.K., Tavolari, S., Huang, T., Chan, M.W., Marini, F.C., Rosol, T.J., et al. (2008). Fibroblasts isolated from common sites of breast cancer metastasis enhance cancer cell growth rates and invasiveness in an interleukin-6-dependent manner. Cancer Res. *68*, 9087–9095.

Tian, D.S., Peng, J., Murugan, M., Feng, L.J., Liu, J.L., Eyo, U.B., Zhou, L.J., Mogilevsky, R., Wang, W., and Wu, L.J. (2017). Chemokine CCL2-CCR2 signaling induces neuronal cell death via STAT3 activation and IL-1beta production after status epilepticus. J. Neurosci. *37*, 7878–7892.

van Steensel, L., Paridaens, D., Dingjan, G.M., van Daele, P.L., van Hagen, P.M., Kuijpers, R.W., van den Bosch, W.A., Drexhage, H.A., Hooijkaas, H., and Dik, W.A. (2010). Platelet-derived growth factor-BB: a stimulus for cytokine production by orbital fibroblasts in Graves' ophthalmopathy. Invest. Ophthalmol. Vis. Sci. *51*, 1002–1007.

Yang, X., Lin, Y., Shi, Y., Li, B., Liu, W., Yin, W., Dang, Y., Chu, Y., Fan, J., and He, R. (2016). FAP promotes immunosuppression by cancer-associated fibroblasts in the tumor microenvironment via STAT3-CCL2 signaling. Cancer Res. *76*, 4124–4135.

ISCI, Volume *19*

Supplemental Information

Paracrine Crosstalk between Fibroblasts and ER^+ Breast Cancer Cells Creates an IL1β-Enriched Niche that Promotes Tumor Growth

Sumanta Chatterjee, Vasudeva Bhat, Alexei Berdnikov, Jiahui Liu, Guihua Zhang, Edward Buchel, Janice Safneck, Aaron J. Marshall, Leigh C. Murphy, Lynne-Marie Postovit, and Afshin Raouf

Transparent Methods

Tissue collection and processing

Estrogen receptor positive (ER^+) breast tumours (>2cm) and matching tumour-adjacent tissue (TAT) samples were obtained from patients undergoing mastectomy surgery without any prior treatment. TAT samples were obtained 3-6 cm away from the primary tumour margin and declared disease-free and histologically benign by a pathologist. Contralateral tumour-free breast tissue was also obtained from patients with ER^+ tumours undergoing prophylactic bilateral mastectomy. As a source of normal breast tissue, reduction mammoplasty samples were obtained. Samples were transported to the laboratory in transport medium as previously described (Basak et al., 2015; Chatterjee et al., 2018; Chatterjee et al., 2015) for further processing. All samples were obtained with written informed patient consent according to protocols approved by the University of Manitoba's Research Ethics Board. Tissue samples were dissociated enzymatically for 16 hours in dissociation media as described previously. Cell pellets were re-suspended in 6% dimethylsulfoxide (DMSO)-containing fetal bovine serum (FBS)-supplemented medium for liquid nitrogen storage.

Isolation of different subset of cells from the breast tumours

Single cell suspensions from fresh or frozen tumour samples were depleted of immune and endothelial cells by magnetically separating $CD45^+CD31^+$ (Lin-) cells using EasySep™ Human Biotin Selection Kit (StemCell Tech.) and were cryogenically preserved in liquid Nitrogen. Subsequently, the $EpCAM^+$ breast cancer cells were isolated using EasySep™ Human EpCAM Positive Selection Kit (StemCell Tech.). Isolated $EpCAM^+$ breast cancer cells (BCCs) were either cryogenically preserved or used right away. Before freezing, viability for each cell fraction was assessed by propidium iodide (PI) staining and flow cytometric analysis. The $EpCAM^-$ cell fraction was used to generate tumour-associated fibroblasts (TAFs) lines as described previously (Chatterjee et al., 2018).

Patient-derived organoid cultures

50 µl of liquid growth factor-reduced matrigel (BD Biosciences) was placed in each well of a 96-well plate and 50 µl of PBS added on top to prevent evaporation while the gels were allowed to polymerize at 37°C for 30 minutes in a humidified chamber. Between $3x10^4$-$5x10^4$ cells from the primary $EpCAM^+$ BCCs and *in vitro* expanded fibroblasts were mixed with 200µl organoid media (SF7 growth media (Stingl et al., 2001)supplemented with 10µM Y27632 and 10µM SB431542) (both from StemCell Tech.) and placed on top of polymerized matrigels either alone or together at 1:1 ratio with NAFs or TAFs and plates were transferred to a humidified 37°C, 5% CO_2 incubators

at ambient O_2. For the purposes of these experiments, we successfully generated 11 patient-derived organoids from 17 individual ER+ breast tumour samples.
The medium was changed every 3 days and after 10 days, gels were dissolved with dispase and organoids were made into single-cell suspension as described previously (Chatterjee et al., 2018). For some experiments, organoid cultures also contained $CD45^+CD31^+$ cell fraction from the tumours at 1:1:1 ratio (50,000 of each cell type) with $EpCAM^+$ BCCs and TAFs obtained from the same original tumour. In some experiments, organoid media were supplemented with recombinant CCL7 (1-10ng/mL), IL6 (1-10ng/mL), IL8 (1-10ng/mL), TGFα (1-10ng/mL), MDC (1-10ng/mL), GROα (1-10ng/mL), IL1RA (1-10ng/mL), IL1β (10pg-1ng/mL), and PDGF-BB (500pg-10ng/mL) (all from Sigma). Some co-cultures were treated with 4-hydroxytamoxifen (Tam, at, 100nM and 1μM, Tocris Biosciences), IL1RA (IL1R1 receptor antagonist, 100ng/mL, Biolegend) and SU16f (selective PDGFRβ blocker, 10μM, Tocris Biosciences) (Cheng et al., 2011; Jiang et al., 2017; Lee et al., 2014).
In some experiments MCF7 cells were placed in organoid cultures with SF7 growth media and After 48 hr, media were replaced with fresh media containing different concentrations (50nM-1μM) of Tam and cultured for an additional 8 days with media changes every 3 days. Subsequently, gels were dissolved and made into single-cells as described (Basak et al., 2015; Chatterjee et al., 2018) and cell viability determined via PI dye retention using flow cytometry.

Primary fibroblast cultures

Fibroblasts from the Tumour (TAFs), TAT (TAT-Fs), and normal breast reduction (NAFs) samples were obtained by expanding the $EpCAM^-$ subset of dissociated tumour cells in adherent 2 dimensional (2D) cultures as described before (Chatterjee et al., 2018). Briefly, $EpCAM^-$ cells were cultured in DMEM/F12 media supplemented with 10% FBS at 37°C and cultured to 70-75% confluency. All fibroblast lines were passaged at least twice to obtain near homogeneity and presence of mesenchymal markers (CD73, CD90, CD105, CD13 and FSP1/S100A4) (all from BD-Biosciences) and absence of epithelial (EpCAM) (StemCell Technologies), endothelial (CD31) (e-biosciences) and immune (CD45) (BD-Biosciences) cell markers was examined by flowcytometry.

Breast cancer cell lines

ER^+ breast cancer cell lines MCF7 and T47D and the triple negative MDA-MB-231 cells were maintained in 5% FBS containing DMEM or 10% FBS containing RPMI or 10% FBS containing DMEM media growth media respectively. MCF7 and T47D cell lines were authenticated recently (October, 2016) using STR analyses (Genetica Cell Line Testing, Labcorp, Burlington, NC, USA). All experiments were carried out using stocks between passages 2-5. All cells were grown upto 70-75% confluency before passaging. For some experiments, MCF7 and T47D cells were co-cultured with NAFs, TAT-Fs, TAFs, or contralateral non-tumour containing breast-fibroblasts (CNTB-Fs) at 1:1 ratio ($5x10^4$-$1x10^5$ of each cell type) for up to 10 days in 2D adherent cultures.

For other experiments, MCF7 and T47D cells were grown in 3D matrigels and treated with recombinant TGFα, MDC, IL1RA, IL1β and PDGF-B (all from sigma) for 8 days.

Conditioned media (CM) collection

Primary EpCAM$^+$ BCCs ($1x10^5$) were placed in organoid cultures either alone or with NAFs or TAFs ($1x10^5$) and after 48 hr medium was replaced with 100 µl of fresh medium which was then collected either after 48 hr or 8 days (as control for long-term organoid cultures). The collected media (conditioned media, CM) were centrifuged for 5 mins at 1200 rpm and supernatants were stored at -80°c. Fibroblast-only conditioned media were also collected. For some experiments CM were obtained from the CD45$^+$CD31$^+$ cell fraction of breast tumours grown in matrigel for 8 days. For some other experiments, MCF7 and T47D cells were cultured in 2D either alone or with different fibroblasts for upto 75% confluence when fresh medium was added and CM were collected after 48hr.

Cytokine ELISA array

CM collected after 8 days from the EpCAM$^+$ BCCs and NAFs in organoid cultures either alone or in co-culture were sent to Eve Technologies for 65-plex human cytokine/chemokine enzyme-linked immunosorbent assay (ELISA) analysis. For some experiments, cytokine array analysis was done on CM collected from the CD45$^+$CD31$^+$ cell fraction of the tumours grown in matrigel for 8 days. For experiments described in Fig. 4C, MCF7, T47D, and NAF cells were grown in 2D adherent cultures and CM were collected from each culture after 48hr (Fig. 4C, CM1). TAF-CM was placed on MCF7 or T47D for 48hr (Fig. 4C, CM2). CM1 and CM2 samples were sent for cytokine/chemokine ELISA array analysis (Table S2). Each cytokine/chemokine examined was accompanied with a standard curve and cytokine expression values are the average of 3 biological replicates.

Colony-forming cell assays

Colony-forming cell (CFC) assays were performed as previously described (Basak et al., 2015; Chatterjee et al., 2018; Chatterjee et al., 2015). Briefly, 5,000 Lin- cells from breast reduction samples or dissociated organoids from matrigels were plated together with 80,000 irradiated mouse NIH 3T3 cells in SF7 medium supplemented with 5% FBS. After 7–10 days, colonies were fixed with a 1:1 (vol/vol) mixture of methanol and acetone on ice and then stained with crystal violet (Sigma). Colony types and numbers were obtained using a bright field microscope.

Flow cytometric analyses

Single-cell suspensions obtained from the $EpCAM^+$, $CD45^+CD31^+$ subset of ER^+ primary tumours were pre-blocked with 2% FBS-containing Hank's Balanced Salt Solutions (HBSS) supplemented with 10% human serum for 15 minutes. The $EpCAM^+$ cells were labelled with anti-human EpCAM (StemCell Technologies) and MUC1 (Millipore) antibodies and the $CD45^+CD31^+$ cells were stained with LIVE/DEAD™ Fixable Aqua Dead Cell Stain Kit (Thermo Fischer) and anti-human CD45, CD3, CD19, CD14 and CD56 antibodies (all from BD Biosciences). NAFs and TAFs were stained with anti-human CD73, CD90, CD105, CD13 (all from BD Biosciences) and IL1R1 (Invitrogen) antibodies. For some experiments, single cell suspensions from organoid-enriched fractions were labeled with anti-human CD49f (Biolegend) and EpCAM antibodies. To obtain MCF7 and T47D cell numbers in fibroblast co-cultures, cells were stained with anti EpCAM antibody. For all experiments, propidium iodide (PI, Sigma) exclusion was used to identify viable cells.
Intracellular flow cytometry was performed as described (Basak et al., 2015) to detect CK5, CK14, CK8/18, αSMA, p63 and ERα expression in the $EpCAM^+$ BCCs and the expression of FSP1 in the fibroblasts. For analyzing cytokine secretion (IL1β, PDGF-BB, CCL7, IL6 and IL8), cells were first incubated with Brefeldin A (e-Biosciences) for 6 hr before fixing and stained with different primary antibodies. The flow cytometry data were analyzed using the FlowJo software (BD-Biosciences).

Quantitative real-time PCR

Total RNA was extracted from fresh, FACS-sorted non-cultured or cultured cells using the Trizol reagent (Invitrogen). cDNA was prepared from 1 μg of RNA using the Maxima cDNA synthesis kit (Thermo Fisher) and then used as a template for PCR. Transcript expression of specific genes was obtained using gene-specific primers. Relative expression levels of specific transcripts were calculated by normalizing to housekeeping genes (*GAPDH, TFRC* and *HPRT*) transcript levels.

Western blot analysis

Fibroblasts were grown in 2D culture to 70-75% confluency and protein extracts were prepared using 2% sodium dodecyl sulfate (SDS) buffer with complete protease inhibitor tablets (Roche Diagnostics). Western Blots were carried out using standard protocols with 70-90 μg of total protein. Protein expression was determined using anti PDGFRα (Santa Cruz Biotech.), PDGFRβ (Santa Cruz Biotech.), STAT3 (Cell Signaling Tech.), phosphorylated STAT3 (pSTAT3, Cell Signaling Tech.), and beta actin (Sigma) antibodies by chemiluminescence. The expression level of each protein was determined using beta actin expression as loading control.

Clinical outcome and gene expression analysis

To assess the relationship between *IL1β* and *PDGFB* gene expression and patients' risk/survival in The Cancer Genome Atlas (TCGA) invasive breast carcinoma cohorts (962 cases; build July 2016), we used the SurvExpress tool (http://bioinformatica.mty.itesm.mx:8080/Biomatec/SurvivaX.jsp). A prognostic index (PI) was generated from the most up-to-date TCGA invasive breast carcinoma data set using *IL1β* and *PDGFB* gene expression. PI is the linear component of the Cox model, PI=β1x1+ β2x2+...+βpxp, where xi is the gene expression value and the βI can be obtained from the Cox fitting. Each βI can be interpreted as a risk coefficient. The risk groups are generated by dividing the ranked order PI values into 2 groups, low risk and high risk group (i.e. higher PI values). This achieved by using the medial PI score to divide the data set into 2 groups. The log-ranked test of differences between risk groups, hazard ratio estimate, and gene expression in high and low risk groups was obtained. For *IL1β* and *PDGFB*, the software determined the prognostic index values which were used to divide the dataset into high and low-risk groups; overall Survival was used as clinical endpoint.

Animal experiments

ER+ MCF7 breast cancer cells ($1x10^6$ cells) and tumour-associated fibroblasts ($1x10^6$ cells) were mixed and injected intraductally in to 6-8 weeks old non-obese diabetic (NOD)-scid IL2Rgamma^{null} (NSG) female mice with estrogen pellet implants (17β-ESTRADIOL pellets (1.7 mg, 60-day release, Innovative Research of America as in (Quail et al., 2012)). All experiments involving animals were approved by the Animal Use Subcommittee at the University of Alberta (AUP00001288 and AUP00001685). Two days after injection, mice (6 mice per experimental arm) were treated daily with an IL1β receptor blocker Anakinra (400mg/kg of body weight/per day injected subcutaneously) or a PDGF receptor blocker SU16F (10mg/ kg of body weight/day via gastric gavage) or combination of both drugs or DMSO as vehicle control. After 2 weeks, mice were sacrificed, tumour xenografts were excised and weighed, and formalin-fixed sections from each tumour was stained with hematoxylin and eosin (H&E).

Cell density quantification of H&E sections

Quantification of cell density (i.e. cell-free areas) in the H&E sections from the tumour xenografts was done using QuPath v0.1.2 (https://qupath.github.io/QuPath-v0.2.0) software in conjunction with the ImageJ (https://imagej.net) essentially as described (Bankhead et al., 2017). The software's manual annotation tool was used to select the total tumour area and the *SLIC superpixel segmentation* command was applied to subdivide the annotated region into 'superpixels' (yellow lines, Supplementary Figure 5I). Intensity features were obtained for each superpixels along with Haralick texture features(Bankhead et al., 2017). A two-way random trees classifier was trained to distinguish between area with cells (superpixel segments) and cell-free area (no cell nucleus). The regions with cells and cell-free area were manually curated for each H&E image and annotated. This classification was then applied to all H&E images. The ratio of cell-free area to total area was calculated and used as a surrogate measure of cell density within each xenograft.

Statistical Analysis

The ANOVA and student T-tests were performed using the GraphPad Prism 7.02 program (San Diego, CA).

Supplementary References

Bankhead, P., Loughrey, M.B., Fernandez, J.A., Dombrowski, Y., McArt, D.G., Dunne, P.D., McQuaid, S., Gray, R.T., Murray, L.J., Coleman, H.G.*, et al.* (2017). QuPath: Open source software for digital pathology image analysis. Scientific reports *7*, 16878.

Basak, P., Chatterjee, S., Weger, S., Bruce, M.C., Murphy, L.C., and Raouf, A. (2015). Estrogen regulates luminal progenitor cell differentiation through H19 gene expression. Endocr Relat Cancer *22*, 505-517.

Chatterjee, S., Basak, P., Buchel, E., Safneck, J., Murphy, L.C., Mowat, M., Kung, S.K., Eirew, P., Eaves, C.J., and Raouf, A. (2018). Breast Cancers Activate Stromal Fibroblast-Induced Suppression of Progenitors in Adjacent Normal Tissue. Stem cell reports *10*, 196-211.

Chatterjee, S., Laliberte, M., Blelloch, S., Ratanshi, I., Safneck, J., Buchel, E., and Raouf, A. (2015). Adipose-Derived Stromal Vascular Fraction Differentially Expands Breast Progenitors in Tissue Adjacent to Tumors Compared to Healthy Breast Tissue. Plastic and reconstructive surgery *136*, 414e-425e.

Cheng, F., Pekkonen, P., Laurinavicius, S., Sugiyama, N., Henderson, S., Gunther, T., Rantanen, V., Kaivanto, E., Aavikko, M., Sarek, G.*, et al.* (2011). KSHV-initiated notch activation leads to membrane-type-1 matrix metalloproteinase-dependent lymphatic endothelial-to-mesenchymal transition. Cell host & microbe *10*, 577-590.

Jiang, Y., Berry, D.C., Jo, A., Tang, W., Arpke, R.W., Kyba, M., and Graff, J.M. (2017). A PPARgamma transcriptional cascade directs adipose progenitor cell-niche interaction and niche expansion. Nature communications *8*, 15926.

Lee, E., Pandey, N.B., and Popel, A.S. (2014). Lymphatic endothelial cells support tumor growth in breast cancer. Scientific reports *4*, 5853.

Quail, D.F., Zhang, G., Walsh, L.A., Siegers, G.M., Dieters-Castator, D.Z., Findlay, S.D., Broughton, H., Putman, D.M., Hess, D.A., and Postovit, L.M. (2012). Embryonic morphogen nodal promotes breast cancer growth and progression. PLoS One *7*, e48237.

Stingl, J., Eaves, C.J., Zandieh, I., and Emerman, J.T. (2001). Characterization of bipotent mammary epithelial progenitor cells in normal adult human breast tissue. Breast Cancer Res Treat *67*, 93-109.

Supplementary Figure Legends

Supplementary Figure 1 (A-G) related to Figure 1. Maintenance of primary ER^+ breast cancer cells in organoid cultures and proliferation of MCF7 and T47D in co-cultures

(A) Expression of basal and epithelial cell markers was measured in the primary $EpCAM^+$ breast cancer cells (BCCs) before and after organoid culture for 10 days. Data from 3 different samples are shown as dot plots. (B) Expression of mesenchymal and fibroblast markers was measured in fibroblasts obtained from normal breast reduction tissues after 2 passages. Data from 5 different samples are shown as dot plots. (C) $EpCAM^+$ BCCs obtained from 11 different ER^+ tumour samples were grown in organoid cultures for 10 days and cell numbers are plotted as box and scatter plots. (D) Normal-associated fibroblast (NAF) cell numbers before and after 10-day organoid cultures are shown as box and scatter plot. Data from 6 samples were plotted. (E) 2D adherent co-cultures were initiated with estrogen receptor (ER^+) breast cancer cell lines (MCF7, T47D) and NAFs or contralateral non-tumour breast tissue (CNTB-F) and number of viable $EpCAM^+$ cancer cells (E & F) or the $EpCAM^-$ fibroblasts (G) were quantified by flow cytometry at the beginning (input) and after 3, 5 and 10 days (output). Average cell numbers and standard error of the mean (SEM) from 3 independent experiments are represented in the line graphs. (***P < .0005 and ****P < .00005)

Supplementary Figure 2 (A-F) related to Figure 2. IL1β inhibits normal breast epithelial progenitor expansion. Transcript expressions of *IL1β* target genes were assessed by qRT-PCR in (A) normal-associated fibroblasts (NAFs), and (B) MCF7 cells treated with recombinant IL1β (rIL1β) for 6 hrs. Average gene expression and standard error of the mean (SEM) from 3 independent experiments are depicted in the bar graphs. (C) Single-cell suspensions from reduction mammoplasty samples were placed in organoid culture and treated with recombinant rIL1β for 8 days and acinar structure formation was examined and photographed. Scale bars represent 400μm. (D) EpCAM and CD49f expression in cells obtained from (C) was examined by flow cytometry. A representative plot is shown and the average percentage of cells in each gate and SEM from 4 independent samples is shown in each quadrant. (E) Total number of viable cells and (F) colony forming cell (CFC) yields are depicted in bar graphs. Average cell numbers and CFC yield with SEM from 4 independent experiments are depicted in the bar graphs. (*P < .05, **P < .005, ***P < .0005 and ****P < .00005)

Supplementary Figure 3 (A-E) related to Figure 3. Fibroblasts from tumour-adjacent tissue (TAT-F) and contralateral breast tissue (CNTB-F) show similar mechanism of IL1β induction in co-cultures. (A) TATFs and CNTB-Fs express similar to NAFs *IL1β* transcript level. (B) *IL1β* transcript expression was measured in TATFs, CNTB-Fs and NAFs co-cultured with MCF7 or T47D cells for 10 days. (C) TATFs, CNTB-Fs and NAFs were treated with conditioned media (CM) obtained from either the co-cultures with MCF7 or T47D cells or breast cancer cells

only cultures for 6 hr and *IL1β* transcript levels were measured. The data is represented as bar graphs with Mean ± SEM from 3 independent experiments. (D) MCF7 and (E) T47D cells were placed in 2 dimensional co-cultures with tumour-adjacent breast tissue-associated fibroblasts (TATFs), or matching contralateral none tumour containing breast fibroblasts (CNTB-Fs) or NAFs for upto 10 days. Expansion of breast cancer cells in these cultures were measured as the number of viable $EpCAM^+$ via flowcytometry at the beginning (input) and on the indicated days (output). All the data is represented either as bar graphs or line graphs with Mean ± SEM from 3 independent experiments. (*P < .05, **P < .005, ***P < .0005 and ****P < .00005)

Supplementary Figure 4 (A-H) related to Figure 4. Normal breast epithelial cells do not produce PDGF-BB in co-cultures with NAFs. (A) IL1R1 expression in NAF, MCF7, and T47D was measured by flow cytometry. (B) IL1β protein expression as measured by cytokine ELISA array in CM from NAFs, $EpCAM^+$ primary normal breast epithelial cells or organoid co-cultures of both cells types. (C) NAFs were treated with CM2 generated from NAFs and $EpCAM^+$ normal epithelial cell interaction for 6 hr and *IL1β* transcript level was measured by qPCR. (D) $EpCAM^+$ normal breast epithelial cells were treated with CM from NAFs for 6hrs and *PDGFB* transcript expression was measured by qPCR. (E) Primary ER+ tumour cells treated with recombinant PDGF-BB for 6hrs, IL1β transcript expression was measured and plotted. (F) NAFs were treated with either recombinant PDGF-BB or vehicle control for 5 days and number of viable (propidium iodide negative) cells was obtained by flow cytometry. (G) NAFs were placed in organoid cultures and treated with escalating doses of SU16f for 48hrs, followed by the addition of conditioned media from primary ER+ breast cancer cells and NAFs (CM2) for 6hrs and IL1β transcript levels were quantified. (H) NAFs were placed in organoid cultures for along with escalating doses of SU16f and cell numbers were counted after 5 days and plotted. All the data are represented as bar graphs with Mean ± standard error of the mean from 3 independent experiments. (*P < .05, **P < .005, ***P < .0005 and ****P < .00005)

Supplementary Figure 5 (A-H) related to Figure 6. TAFs induce proliferation of breast cancer cells through similar fibroblast-initiated mechanisms. (A, B) 2D adherent co-cultures were initiated with $EpCAM^+$ ER^+ breast cancer cell lines (MCF7, T47D) and NAFs and/or TAFs. Total numbers of viable $EpCAM^+$ tumour cells were measured by flow cytometry at the beginning (input) and on indicated days. (C) Total numbers of viable $EpCAM^-$ fibroblasts were also measured at the beginning (input) and after 5 days of cultures. (D) TAFs were treated with either recombinant PDGF-BB or vehicle control for 5 days and numbers of viable cells were measured by flow cytometry. (E) IL1R1 expression in TAF was measured by intracellular flow cytometry. (F) Expression levels of CCL7, IL6 and IL8 were measured in TAF through intracellular flow cytometry and immunofluorescence analysis. Scale bars represent 200μm. All the data are represented as bar graphs with Mean ± SEM from 3 independent experiments (*P < .05, **P < .005, ***P < .0005 and ****P < .00005). (G) Cox fitting and prognostic indicators were used to

generate risk groups from The Cancer Genome Atlas (TCGA) by the SurvExpress online tool. Kaplan-Meier curves of risk group prediction across the TCGA data set are shown. Red line represents high risk and green line represents the low risk group. (H) *PDGFB* and *IL1β* expression in the high risk and low risk group based on prognostic index is shown. (I) Mixture of MCF7 and TAFs were used in an orthotopic mouse tumour model to generate tumours. Mice were either treated with Anakinra (Ana), SU16F (Su), Ana+Su, or vehicle control. Cell-free areas of H&E sections from each tumour was obtained and analyzed as described in the supplementary materials and methods section. Representative areas of analysis from each xenograft section is shown. Areas containing cells (MCF7 and TAFs) are selected (yellow lines) and the ration of cell-free area in each xenograft section was normalized to the total tumour area.

Supplementary Figure 6 (A-F) related to Figure 7. Characterization of ER^+BCC-associated $CD45^+CD31^+$ cells. (A) Tumour-associated fibroblasts (TAFs) or (B) $CD45^+CD31^+$ cells from the primary estrogen receptor positive breast tumours were put into organoid cultures and the number of viable (propidium iodide negative, PI^-) cells after 10 days were obtained by flow cytometry. Line graphs from 3 independent samples are shown. (C) Cytokine ELISA array analysis identified 65 different cytokines secreted by ER^+BCC-associated $CD45^+CD31^+$ cells (also, Table S3). Average from 3 biological replicates and standard error of the mean (SEM) are plotted as bar graphs. (D) Flow cytometric analysis of the ER^+BCC-associated $CD45^+$ cells revealed presence of different immune cells ($CD3^+$ T, $CD19^+$ B, $CD14^+$ Monocytes and $CD56^+$ NK cells) in the tumour microenvironment. Data from 5 independent samples were plotted as dot plots. (E) pi-chart showing different cytokines secreted by different immune cell subsets in the ER^+BCC-associated $CD45^+CD31^+$ cells. (F) MCF7 cells were grown as organoids and treated with different concentrations of tamoxifen (Tam) for 8 days and viable (PI^-) cell numbers were determined by flow cytometry. The data are represented as bar graphs from 3 independent experiments as Mean ± SEM. (*P < .05, **P < .005, ***P < .0005 and ****P < .00005)

Supplementary Figure 1 (A-G) related to Figure 1

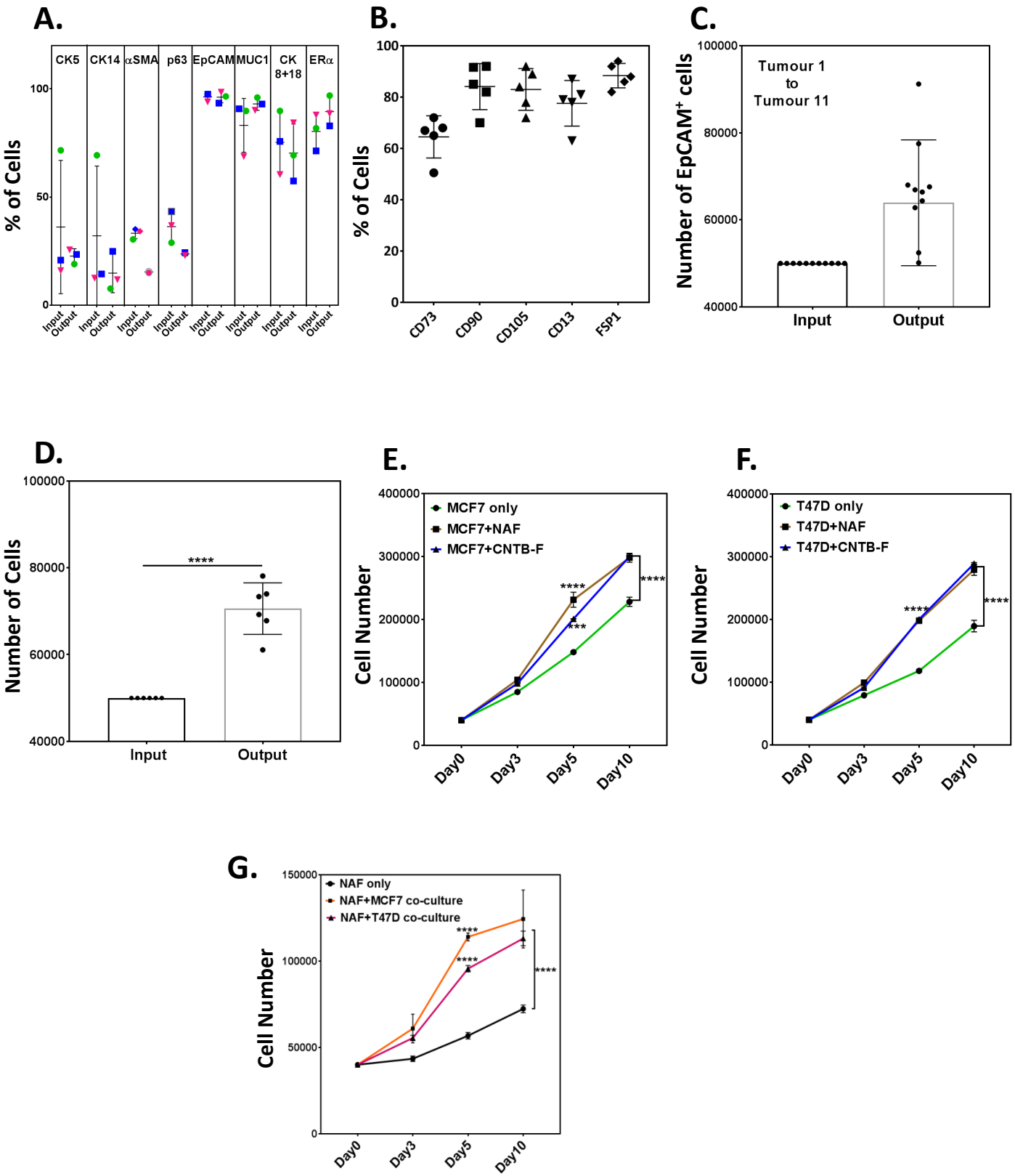

Supplementary Figure 2 (A-F) related to Figure 2

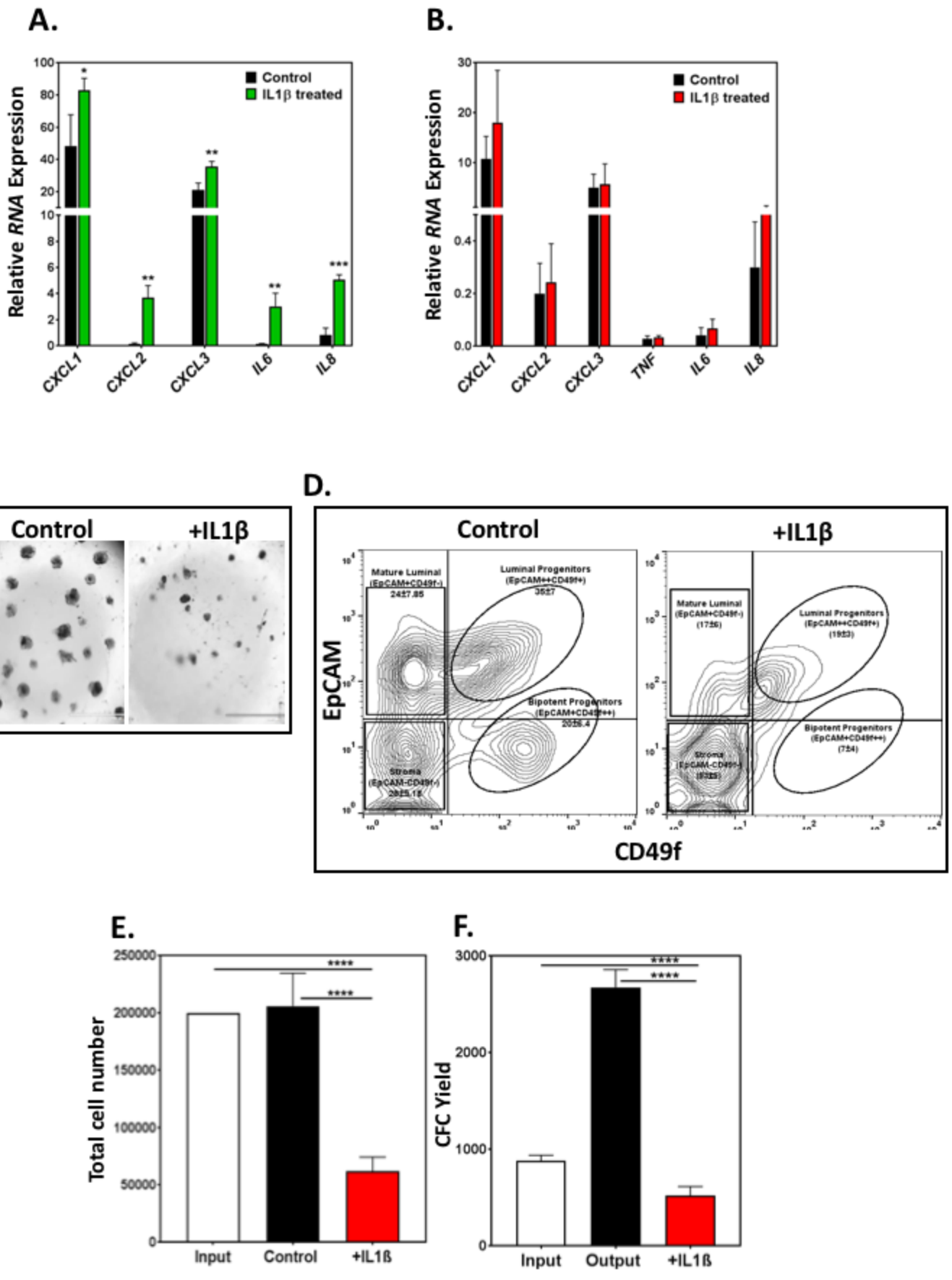

Supplementary Figure 3 (A-E) related to Figure 3

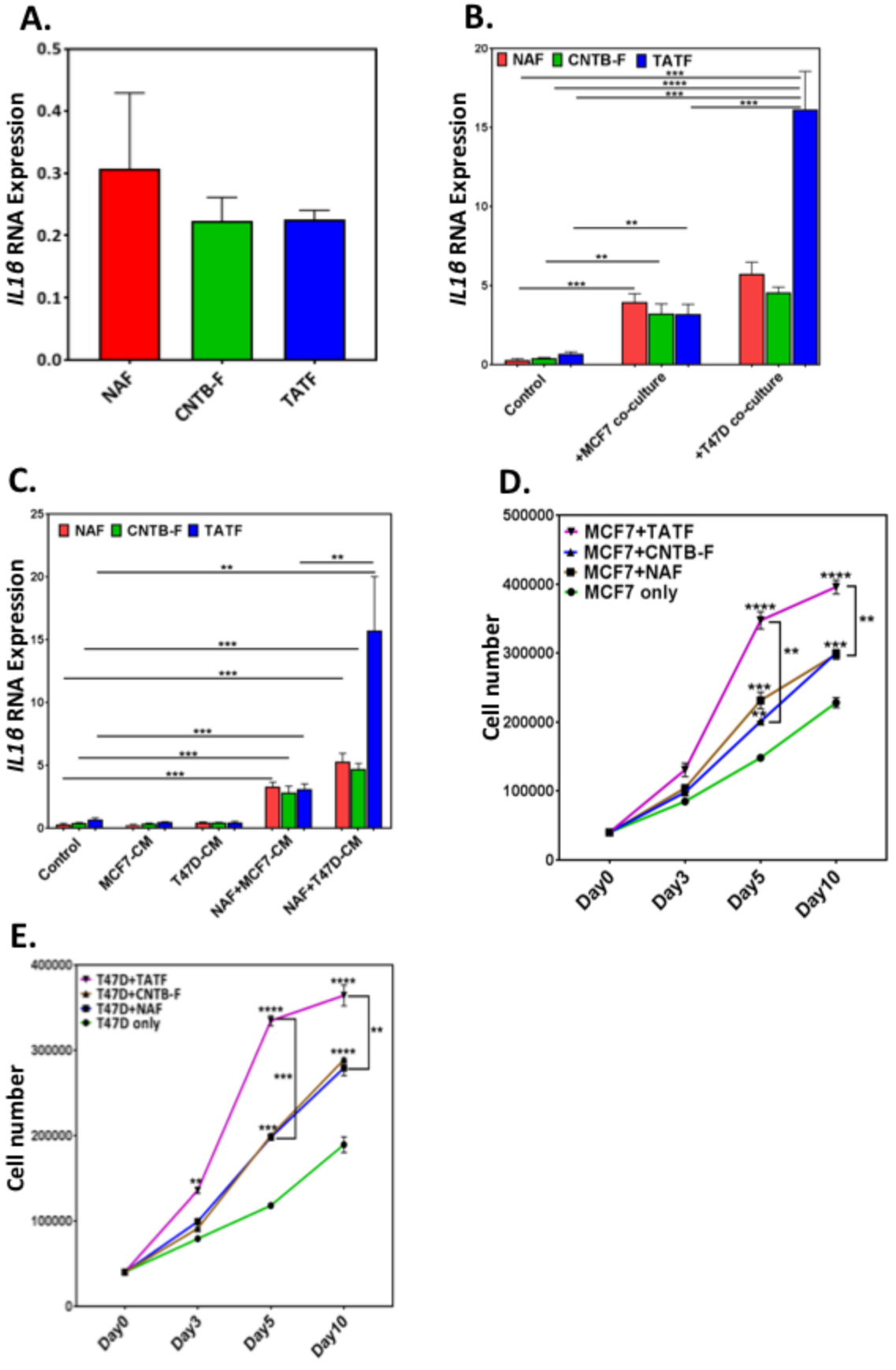

Supplementary Figure 4 (A-H) related to Figure 4

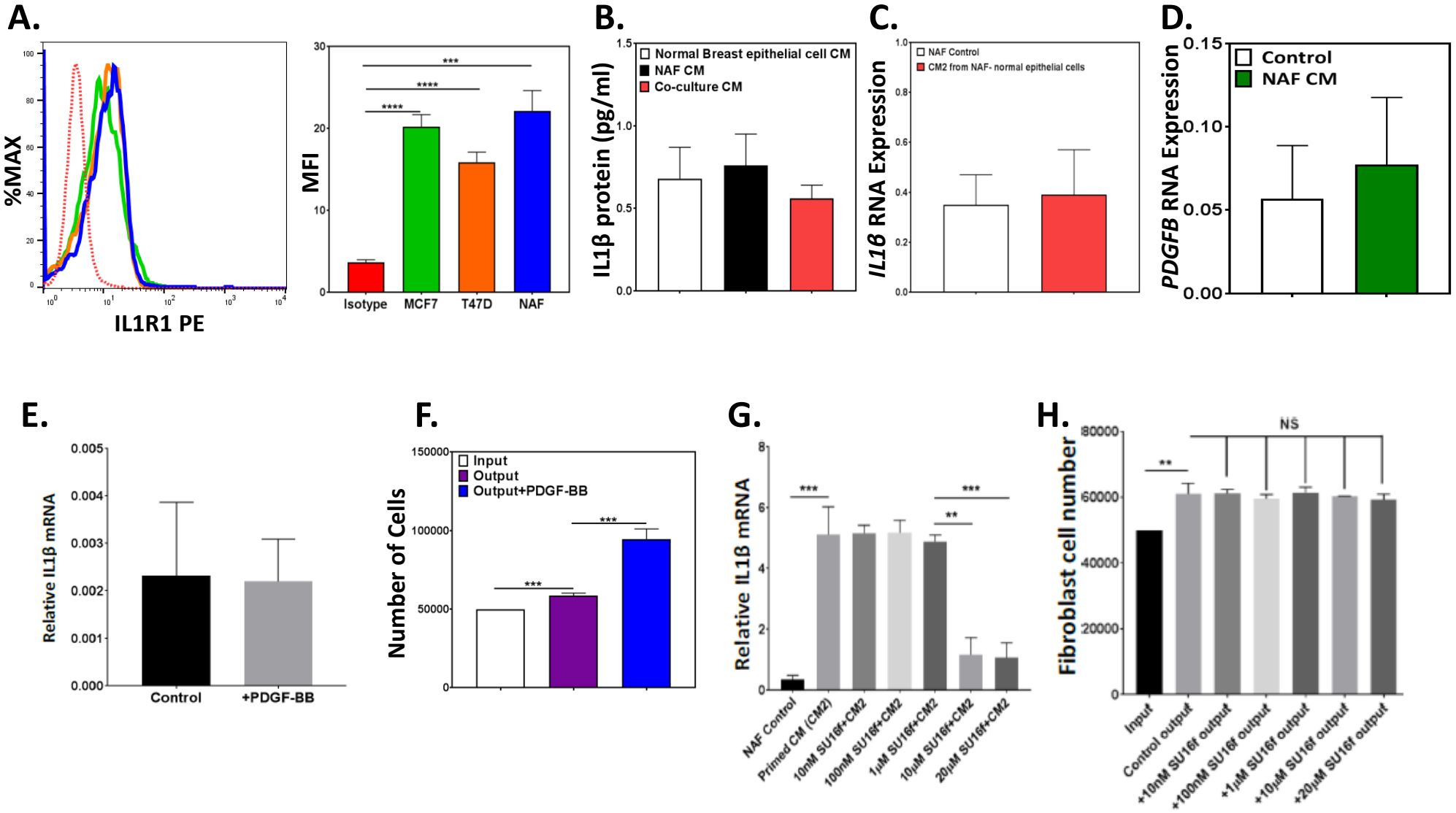

Supplementary Figure 5 (A-H) related to Figure 6.

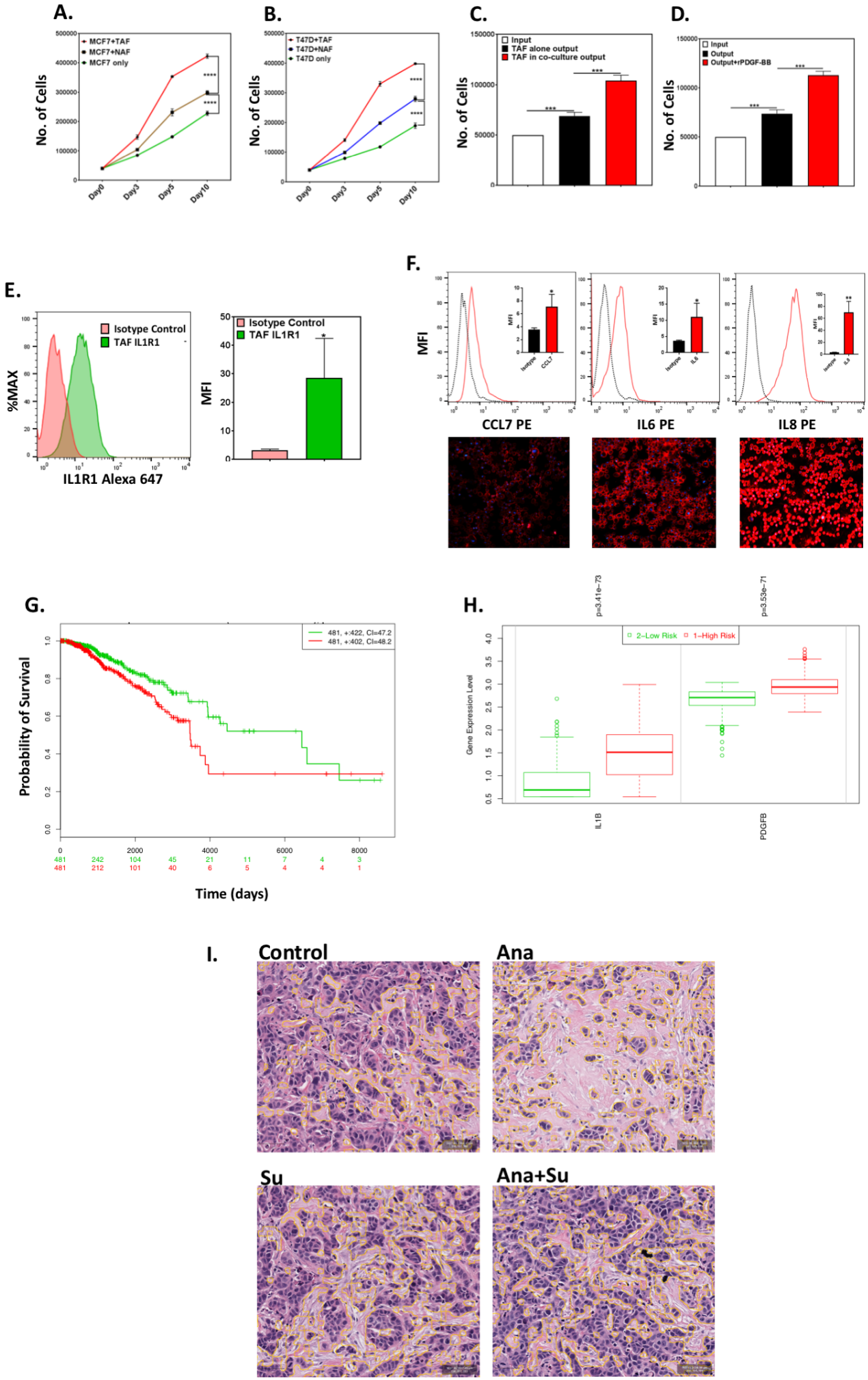

Supplementary Figure 6 (A-F) related to Figure 7